Lithos
December 2019, Volume 350 Pages 105235 (18p.)
https://doi.org/10.1016/j.lithos.2019.105235
https://archimer.ifremer.fr/doc/00773/88507/

Archimer
https://archimer.ifremer.fr

Multi-scale development of a stratiform chromite ore body at the base of the dunitic mantle-crust transition zone (Maqsad diapir, Oman ophiolite): The role of repeated melt and fluid influxes

Rospabé Mathieu [1, 2, *], Ceuleneer Georges [1], Granier Nicolas [1], Arai Shoji [3], Borisova Anastassia Y. [1, 4]

[1] Univ Toulouse, CNRS, IRD, GET,Observ Midi Pyrenees, 14 Ave E Belin, F-31400 Toulouse, France.
[2] Japan Agcy Marine Earth Sci & Technol JAMSTEC, Res Inst Marine Geodynam IMG, 2-15 Natsushima, Yokosuka, Kanagawa 2370061, Japan.
[3] Kanazawa Univ, Coll Sci & Engn, Dept Sci, Kanazawa, Ishikawa 9201192, Japan.
[4] Lomonosov Moscow State Univ, Geol Dept, Moscow 119899, Russia.

* Corresponding author : Mathieu Rospabé, email address : mrospabe@jamstec.go.jp

Abstract :

A stratiform chromite ore body crops out in the lower part of the dunitic mantle-crust transition zone (DTZ) that developed at the top of a mantle diapir in the Maqsad area in the Oman ophiolite. It is made of layers ranging in thickness from a few mm to a maximum of 3 m, and in modal composition from massive to antinodular and disseminated ore. The ore body is about 50 m thick and its lateral extent does not exceed several hundred meters. The layering dips gently to the southeast, parallel to that of the overlying gabbroic cumulates. The chromite composition is typical of a MORB kindred - moderate XCr (100 x Cr/(Cr + Al) atomic ratio), ranging from 48 to 60, and relatively high TiO2 content, ranging from about 0.3 to 0.5 wt% -, a characteristic shared by most lithologies issued from the igneous activity of the Maqsad diapir. The silicate matrix is essentially made of slightly serpentinized olivine with minor clinopyroxene and rare pargasitic amphibole, orthopyroxene and garnet. This strongly contrasts with the nature of the mineral inclusions mostly made of the assemblage amphibole-orthopyroxene-mica, enclosed in the chromite grains and represented in abundance all along the ore body whatever the ore grade. The inclusions demonstrate the involvement of a silica- and water-rich melt and/or fluid, in addition to MORB, in the early stages of chromite crystallization. The chemical composition of chromite, silicate matrix, together with the one of silicate inclusions display well-defined evolutions vertically along the stratiform chromitite. At the scale of the ore body, the compositional trends are independent of the ore concentration but the major kinks in these trends are well-correlated with levels of magmatic breccias. This shows that abrupt chemical changes can be attributed to sudden melt fluids injection events followed mainly by melt-fluid-rock interaction and in a lesser extent by quieter evolution by fractional crystallization. At the thin section scale, second order chemical variations, essentially in the Mg# (100 x Mg/(Mg + Fe2+) atomic ratio) of chromite and Fo of olivine, are clearly attributable to re equilibration between these two solid phases, possibly in the presence of an interstitial melt/fluid.

Please note that this is an author-produced PDF of an article accepted for publication following peer review. The definitive publisher-authenticated version is available on the publisher Web site.

Highlights

► The Maqsad dunitic transition zone (Oman ophiolite) hosts a stratiform chromitite. ► The matrix (ol, cpx) strongly contrasts with silicate inclusions (opx, amph, mica). ► Vertical chemical evolutions along the ore body correlate to magmatic breccias. ► Melt injections (breccias) controlled the hybridization between contrasted melts.

Keywords : Oman ophiolite, Chromite, Stratiform chromitite, Melt hybridization, Dunitic mantle-crust transition zone

Please note that this is an author-produced PDF of an article accepted for publication following peer review. The definitive publisher-authenticated version is available on the publisher Web site.

1. Introduction

The fate of chromium from its mantle source and its concentration by the crystallization and accumulation of chromite in cooling magma bodies is a long-standing poorly understood process of the magmatic history of mafic and ultramafic rocks (e.g. Bowen, 1928; Lombaard et al., 1956; Stoll, 1958), and is still the matter of intense discussions (cf. Arai and Miura, 2016 and references therein). Different mechanisms were proposed to account for the formation of massive chromitites in crustal magma chambers, following the crystallization from a chromite-oversaturated basaltic melt in which chromite was the only liquidus phase and by the chromite crystals settling and concentration in layers of variable thickness. Among others processes, the mixing between a basalt saturated in chromite and a more silicic melt, contamination of the basalt by the surrounding felsic crustal rocks, addition of H_2O, increase in the total pressure or fO_2 of the parent magma, saturation in chromite alone in the parent magma following a decrease in the lithostatic pressure (e.g. Irvine, 1975, 1977a, 1977b; Latypov et al., 2018; Lipin, 1993; Matveev and Ballhaus, 2002; Mondal and Mathez, 2007; Naldrett et al., 2012; Spandler et al., 2005) were proposed. The most popular model consists in the massive chromite crystallization from a melt hybrid between a relatively primitive basalt and a silica-rich melt, issued from the country rock re-melting (Irvine, 1975) or from the same melt at a more evolved, differentiated stage (Irvine, 1977a). Some authors also proposed the involvement of volatile- and sodium-rich melts or

fluids based on the nature of hydrous, Na-rich silicate inclusions in chromite grains (e.g. Borisova et al., 2012; Johan et al., 1983, 2017; McElduff and Stumpfl, 1991; Spandler et al., 2005; Talkington et al., 1984), while in extreme cases chromite may be entirely attributed to hydrothermal processes (Arai and Akizawa, 2014).

Chromitite ore bodies were mainly reported in continental layered intrusions and in ophiolites worldwide, whatever their tectonic setting (i.e. supra-subduction zone or mid-oceanic ridge). Recent sampling in present-day oceans documented cm-thick chromitites associated with abyssal peridotites (Abe, 2011; Arai and Matsukage, 1998; Payot et al., 2014). Silicate inclusions in their chromite grains (chromitites and chromite grains scattered in olivine-rich troctolites) are similar to the ones observed in layered intrusions and ophiolites (Matsukage and Arai, 1998; Tamura et al., 2014). This demonstrates that the formation of chromitite may occur in various magmatic environments involving a wide spectrum of parent melts and a silica-, alkali- and water-rich melt or fluid not necessarily issued from the subduction factory. Accordingly, the topic of the geochemical cycle of Cr has to be addressed by the study of the local processes involved in the formation of a given ore body (surrounding rocks, nature and proportion of the melts/fluids, physical settings, etc.), rather than through the tectonic setting in which the chromitite formed.

Stratiform chromitite ore bodies are among the most impressive expressions of Cr mobilization and fractionation, chromite-seams alternating with harzburgite, dunite, gabbro, orthopyroxenite, norite, anorthosite among other (e.g. Jackson, 1961; Mathez and Kinzler, 2017; Thayer 1960). They were made famous by their occurrence in large (up to few tens to few hundreds km) and thick (up to few km), layered igneous complexes that intruded continental domains through massive magmatic events in old Archean to Proterozoic geological times (e.g. Muskox, Stillwater, Bushveld and Great Dyke among the most studied complexes). Stratiform chromitites of much smaller size were described in ophiolitic

sequences and share many features with chromite-seams in layered intrusions (e.g. texture, lithological associations, silicate inclusions) (e.g. Borisova et al., 2012; Gauthier et al., 1990; González-Jiménez et al., 2014; Lorand and Ceuleneer, 1989; Rahgoshay et al., 1981), such as in Oman where they are restricted to the dunitic mantle-crust transition zone (DTZ) (Augé, 1987; Ceuleneer and Nicolas, 1985), which contrasts with the podiform chromite ore bodies more common in the underlying harzburgitic mantle section. They preserved their igneous structure when they escaped post-crystallization deformation resulting from off-ridge-axis transposition, associated to diverging mantle solid-state flow (Cassard et al., 1981; Ceuleneer and Nicolas, 1985).

The formation of chromitite in the upper mantle beneath oceanic ridges is thought to be closely related to the formation of dunite. As a matter of fact, a reactional dunitic envelope underlines, as a rule, the contact between chromitite and surrounding mantle harzburgites while abundant chromitites also occur within the DTZ (e.g. Arai and Yurimoto, 1994; Cassard et al., 1981; González-Jiménez et al. 2014; Lago et al., 1982). The chromite grains scattered in the DTZ share the same abundant mineral inclusions than the chromite grains from chromitites (e.g. Borisova et al., 2012; Rospabé et al., 2017). Consequently, both dunite and chromitite appear to be, in this context, two associated products formed at the expense of harzburgite following melt- or magma-peridotite reactions (Arai and Yurimoto, 1994; Borisova et al., 2012; Zhou et al., 1994).

In order to better understand the formation of stratiform chromitites beneath oceanic spreading centres, we performed a detailed sampling of an undeformed stratiform chromitite ore body cropping out within the Maqsad DTZ in Oman (Ceuleneer and Nicolas, 1985). Our results highlight that the processes that governed chromite composition are different depending on the scale: chemical re-equilibration at local (thin section) scale, and episodic magmatic influxes at a larger (ore body) scale.

2. The Maqsad area of the Oman ophiolite

The Oman ophiolite is a fragment of the Cretaceous oceanic lithosphere accreted in the Tethys ocean about 95-97 Ma ago (Tippit et al., 1981), detached during an intra-oceanic thrusting event that occurred contemporaneously, soon after or soon before the accretion (Montigny et al., 1988; Rioux et al., 2016, 2013; Warren et al., 2005) and obducted onto the Arabian margin during Maestrichtian times (circa 70 Ma) (Coleman, 1981; Glennie et al., 1973). The precise context of genesis and emplacement of the Oman ophiolite is still debated: a "pure" mid-ocean ridge setting according to some authors (e.g. Coleman, 1981), a subduction zone setting according to others (e.g. Pearce et al., 1981). The spatial distribution, along the ophiolite, of the nature of mafic dikes cross-cutting the harzburgitic mantle section and of lower crustal cumulates shows that both MORB and depleted calc-alkaline series coexisted at the time of the igneous accretion of the Oman ophiolite (Benoit et al., 1999; Clénet at al., 2010; Python and Ceuleneer, 2003).

The Maqsad area is located in the Sumail massif, in the southeastern part of the Oman ophiolite (Fig. 1a). There, a former axial mantle upwelling ("diapir") has been frozen and has been mapped through the study of high-temperature plastic deformation structures in mantle harzburgites (Ceuleneer, 1991; Ceuleneer et al., 1988; Rabinowicz et al., 1987). The Maqsad diapir is less than 10 km large in cross-section but constitutes the central part of a much larger structure: a former spreading segment, about 80 km in length parallel to the paleo-spreading axis (NW-SE) (Python and Ceuleneer, 2003). The segment itself is characterized by mantle dykes (former channels used by partial melts to reach the crust) filled with cumulates of MORB affinity (Benoit et al., 1996; Ceuleneer et al., 1996; Python and Ceuleneer, 2003; Python et al., 2008). This contrasts markedly with the more common situation observed elsewhere in Oman where mantle dykes are essentially filled with crystallization products

151 from the depleted andesitic melts (Python and Ceuleneer, 2003). These andesites can be
152 generated either by the hydrous re-melting of the oceanic lithosphere in a mid-ocean ridge
153 setting (Benoit et al., 1999; Nonnotte et al., 2005), or in a subduction environment (see
154 discussion in Python et al., 2008 and in Python and Ceuleneer, 2003).

155 The dunitic mantle-crust transition zone (DTZ) is particularly well-developed in the
156 Maqsad area, reaching more than 300 m in thickness above the central part of the diapir
157 (Abily and Ceuleneer, 2013; Boudier and Nicolas, 1995; Ceuleneer and Nicolas, 1985).
158 Dunite from the Oman ophiolite DTZ is mainly interpreted as the product of melt-peridotite
159 interaction (e.g. Boudier and Nicolas, 1995; Koga et al., 2001) while its upper part
160 (shallowest 50 m) may be cumulative in origin after olivine fractionation from highly
161 magnesian melts (Abily and Ceuleneer, 2013).

162 The DTZ was a very dynamic environment formed by several processes frozen at
163 various stages of their development, where the current extensive petrological and geochemical
164 variability is the footprints of dunitization (i.e. incongruent dissolution of the mantle
165 harzburgites' orthopyroxene), melt percolation associated with chemical re-equilibration with
166 the surrounding olivine matrix, refertilization by variably evolved melt batches, compaction,
167 syn-magmatic faulting, later low temperature alteration, etc. (Rospabé et al., 2018, 2019).
168 Among the crystallization products in the DTZ dunites, orthopyroxene and amphibole
169 interstitial to olivine grains have been interpreted to indicate that a hydrous component was
170 involved in the formation of dunites (Rospabé et al., 2017). We proposed that the mantle-crust
171 transition zone beneath oceanic spreading centres is the place of hybridization between the
172 uprising (relatively dry) MORB issued from the mantle partial melting (i.e. recorded by the
173 troctolite and ol-gabbro cumulates in the mantle section - Benoit et al., 1996; Ceuleneer et al.,
174 1996; Python et al., 2003), and a hydrated component coming from above, probably seawater-
175 derived. The volatile-, Si-, Na- and trace elements-rich hybrid lithospheric melt formed during

176 or/and contributed to the harzburgite dunitization process (Rospabé et al., 2017, 2018, 2019).
177 The presence of orthopyroxene and amphibole, together with mica, enclosed in chromite
178 grains strongly suggests that such a hybrid melt was involved early in both the formation of
179 dunite and the re-mobilization of chromium at the mantle-crust transition zone (Rospabé et
180 al., 2017; see also Borisova et al., 2012).

181 Chromitite ore bodies are particularly abundant in the Maqsad area, probably resulting
182 from the intense magmatic activity associated to the rise of a hot diapir up to the base of the
183 crust (Ceuleneer and Nicolas, 1985; Ceuleneer et al., 1996). Those cropping out at the top of
184 this structure, in the DTZ, were not deformed as they were not transposed by mantle solid-
185 state flow. This offers a unique opportunity to study the details of magmatic processes related
186 to chromite ore genesis (e.g. Borisova et al., 2012; Leblanc and Ceuleneer, 1991; Rollinson
187 and Adetunji, 2013; Zagrtdenov et al., 2018).

188

189 **3. Description of the studied stratiform chromitite**

190 *3.1. Structuration of the stratiform chromitite*

191 The studied chromitite ore body is located a few tens of metres above the base of the
192 DTZ near the centre of the Maqsad diapir (Fig. 1b; Ceuleneer and Nicolas, 1985). We
193 collected 62 samples (labelled 06OM04-##) along a vertical section (Fig. 2), before the
194 mining operations that started in 2008 (Fig. 3a-b). The stratiform ore body is made of
195 alternating levels of chromite-bearing dunites and chromitite. It reaches about 50 m in
196 exposed thickness (Fig. 2). The layering is near horizontal, slightly dipping to the SE and
197 strictly parallel to the layering of overlying gabbroic cumulates. This supports the view that
198 the stratiform chromitite formed during the same tectonic/igneous episode as the one that built
199 the overlying crust, and that it preserved its primary structure. The lateral extent of the layers
200 cannot be determined precisely due to erosion, but it does not exceed several hundred metres

as revealed by our general survey of this area (Rospabé, 2018; Rospabé et al., 2018). The studied samples preserve delicate igneous textures and display no evidence for post-crystallization deformation (Fig. 3), which is consistent with the fact that the DTZ in the Maqsad area was frozen at the axis of a spreading centre and not transposed by diverging mantle flow (Ceuleneer et al., 1988; Ceuleneer, 1991).

The vertical organization of the stratiform chromitite is characterized by 5 main chromite-rich layers (labelled I to V in Fig. 2), while levels in between are made of more scattered ore within dunite (Figs. 3c-e and 4a-d). We basically observed the global increase of the chromite content upsection, from rich-levels I to V. Massive ore occurs in layers ranging in thickness from a few cm up to 3 m (Fig. 3c) in the upper rich-layers III to V. In between massive layers (and along layers I and II), the texture of the ore is antinodular. The nodules, typically about 5 mm in size, are mostly made of subhedral single olivine crystals, more exceptionally of aggregates of smaller olivine grains embedded in interstitial chromites. The relative modal abundance of chromite and of olivine presents marked variations, gradual at some places defining graded bedding, sharper at other places (Figs. 3d-f and 4c-e). Thin sections observations reveal the absence of solid-state deformation (Fig. 4), and the antinodular texture of chromite is reminiscent of the poikilitic plagioclase and pyroxene encompassing olivine grains in DTZ dunites (e.g. Koga et al., 2001; Abily and Ceuleneer, 2013; Rospabé et al., 2017), although the antinodular texture consists of aggregates of tiny chromite grains surrounding olivine crystals and never form large monocrystals as plagioclase and pyroxenes. No sintering texture was observed in chromite grains.

Magmatic breccias made of cm-sized dunite and wehrlite fragments embedded in chromite are rather common (Figs. 3g-i and 4f), pointing to a quite dynamic environment during the stratiform chromitite formation. Six main brecciated levels, a few cm to a few dm in thickness, were identified along the cross-section: one near its base (1020 m), two in

between altitudes 1030 and 1034 m (intermediate breccias system), then three in between 1046 and 1052 m (higher breccias system) (Fig. 2). They show no systematic correlation with the abundance of chromite in surrounding rocks.

Olivine is the dominant silicate phase constituting the matrix between chromite grains (Figs. 2 and 4g). The serpentinization degree of olivine in this area, and in the surrounding DTZ, is unusually low compared to many other occurrences of chromite and dunite in the mantle-crust transition zone where the degree of serpentinization reaches a higher degree. Our observations of thin section revealed that it doesn't exceed 30%. Clinopyroxene is likewise regularly observed along the entire cross-section (Fig. 2), appearing as cm-sized poikilitic crystals both associated with and hosting chromite grains in disseminated, antinodular or massive ores (Fig. 4h), and impregnating the olivine matrix in surrounding dunitic levels (Fig. 4f). Interstitial orthopyroxene occurs in only two samples (06OM04-12D2, 1041 m, and -19(2), 1049.5 m). Plagioclase is typically absent in the stratiform chromitite, although common as an interstitial phase between olivine grains in the surrounding DTZ dunites (e.g. Abily and Ceuleneer, 2013; Boudier and Nicolas, 1995; Koga et al., 2001; Rospabé et al., 2017, 2018). Among other minor phases, diopside (hybrid between magmatic and hydrothermal clinopyroxene, see Rospabé et al., 2017) is observed in the half lower part of the stratiform chromitite while amphibole and garnet, appearing together above the two highest magmatic breccias at the altitude 1050 m, are restricted to the upper part of the ore body (Fig. 2).

3.2. Distribution of inclusions in chromite

Chromites contain silicate phases in inclusion. Figure 3 represents their relative abundance in each sample, from 0 to 8 following thin sections observation, as a function of the altitude. Two levels show a particularly high abundance of inclusions, corresponding to

levels affected by magmatic breccias above 1030 m (intermediate breccias system) and around 1050 m (higher breccias system). In the second order, the abundance of inclusions is related to the modal content of chromite since at a given level, despite a quite lower amount of inclusion far away from breccias (for example at the altitude 1040 m), it appears that massive ore contains more inclusions in chromite than disseminated ore. It is worth mentioning that no sample got a "score" of 0, meaning that inclusions were observed in all the 62 studied samples, including in dunites that contain only a few percent of disseminated chromite.

The inclusions have a size ranging from a few microns to more than 100 μm and are generally round-shaped (Fig. 5), more rarely square-shaped (e.g. Fig. 5c and g). Their habitus and distribution within a chromite grain are a quite large inclusion at the centre of the grain and/or a corona of several inclusions that suggests they were trapped at the time the chromite grain growth (Fig. 5a, b and f).

The nature of silicate minerals in the inclusions have been determined using the electron probe. The resulting picture is in strong contrast with the silicate matrix. Orthopyroxene, amphibole and mica are by far the most common phases of the inclusions. They are observed all across the ore body independently from the chromite modal content of the host samples and from the location of magmatic breccias (Fig. 2). Orthopyroxene and mica occur as monomineralic inclusions as well as polymineralic assemblages associated, separately or together, with amphibole (Fig. 5c). When occurring as monomineralic inclusions, the host chromite also generally contains other inclusions filled with amphibole, making this latter phase the most abundant silicate inclusion type. Clinopyroxene (as well as diopside) appears only rarely in inclusion, identified in three samples only while it is an important major component of the matrix. They likewise occur as single inclusions or associated with amphibole. Garnet and nepheline were also identified as very minor

component inclusions. The two nepheline are parts of polymineralic inclusions, occurring in two different chromites from the same sample (06OM04-3A) and associated with amphibole as well as with mica in one case (Fig. 5d). Garnet occurs as monomineralic inclusions (Fig. 5e). One inclusion (06OM04-17) displays a composition very rich in silica, aluminium and sodium (see paragraph 4.5.5.) and fits with a mixing between albite and quartz (Fig. 5g). High-Cr chromite inclusions or coronas are occasionally observed. Coronas are found at the contact between silicate single inclusions or assemblages made of amphibole and mica and the host chromite grain. These chromite inclusions and coronas are observed all along the stratiform chromitite and their presence is not related to the chromite modal content of the host sample, although never observed in massive ores, or to the location of magmatic breccias.

4. Mineral compositions

4.1. Analytical note

Major and minor element concentrations in chromite and silicate phases were determined by *in situ* electron probe microanalysis (EPMA) using a Cameca SX50 microprobe with SAMx automation (Géosciences Environnement Toulouse, Université de Toulouse III, Toulouse, France) and a Cameca SXFive FE microprobe (Centre de MicroCaractérisation Raimond Castaing, Toulouse, France). The operating conditions using the Cameca SX50 were an accelerating voltage of 15 kV and beam current of 10 nA for silicate mineral phases and beam current of 20 nA for chromites with a spot size of 4 μm in diameter. The operating conditions when using the Cameca SXFive FE were an accelerating voltage of 20 kV, a beam current of 20 nA and a spot size of 1 μm in diameter for all minerals. The analysis counting time was of 10 s on peak for each element and 5 s on backgrounds on both sides of the peak for each type of minerals (chromite,

hydrous/anhydrous silicates). The two datasets obtained following the using of the two different microprobes were compared; no shift was observed. The following synthetic and natural minerals standards were used: albite (Na), periclase (Mg), corundum (Al), sanidine (K), wollastonite (Si, Ca), pyrophanite (Mn, Ti), hematite (Fe), chromium oxide (Cr), nickel oxide (Ni), sphalerite (Zn) and pure vanadium (V). Oxides concentrations were obtained by correcting nominal concentrations following the PAP data reduction method (Pouchou and Pichoir, 1985). The detection limits are 0.03 wt% for TiO_2, Al_2O_3, Cr_2O_3 and MgO, 0.04 wt% for SiO_2 and Na_2O, 0.05 wt% for CaO and K_2O, 0.06 wt% for V_2O_3 and NiO, and 0.07% for FeO, MnO and ZnO, for all mineral phases analysed. The internal precision (%RSD) is better than 2% for major elements (e.g. Cr_2O_3 in chromite, MgO in olivine, CaO in clinopyroxene), better than 6% for TiO_2 (chromite, clinopyroxene) and better than 30% for minor elements (e.g. NiO in olivine, Na_2O in clinopyroxene). A few selected data are available in Table 1. The whole dataset is provided in Supplementary Material.

4.2. Chromite

Chromites from the stratiform chromitite are Cr- and Al-rich relative to Fe^{3+} (see ternary diagram in Figure 6). They display variable chemical compositions, with averaged per sample XCr (100 × Cr/(Cr + Al) atomic ratio) = 49.0-59.9 (Cr_2O_3 = 39.4-47.1 wt%; Al_2O_3 = 20.7-27.6 wt%), XMg (100 × Mg/(Mg + Fe^{2+}) atomic ratio) = 50.0-69.8, YFe^{3+} (100 × Fe^{3+}/(Cr + Al + Fe^{3+}) atomic ratio) = 1.1-7.8 (4.6 in average), and TiO_2 = 0.25-0.54 wt% (averaged values for each samples) (Fig. 6). Chromite inclusions and coronas have a higher XCr, ranging from 58.3 to 71.5 (Cr_2O_3 = 43.7-52.7 wt%; Al_2O_3 = 14.1-21.3 wt%), a similar to slightly lower XMg (50.5-63.0), and a less variable but globally higher in average YFe^{3+} (4.3-6.3, 5.3 in average). The YFe^{3+} is slightly higher in chromite inclusions (4.9-6.3) than in coronas (4.3-5.9). Chromite inclusions and coronas also display a clear negative correlation

between their TiO_2 content (0.12-0.51 wt%) and their XCr (Fig. 6).

At the scale of the whole ore body (~ 50 m-thick), chromite composition does not vary randomly. Progressive evolutions can be observed vertically (Fig. 7a): (1) the lowest XCr values are restricted around the lower breccia near the altitude 1020 m and do not exceed 55 until the intermediate breccias system (1030-1034 m), then (2) XCr increases continuously to highest values (~60) toward the higher breccias before (3) a reverse decreasing tendency from the altitude 1050 m and within the uppermost part of the ore body. These continuous evolutions from a sample to another are independent of the amount of chromite in host rock at the scale of the whole stratiform chromitite. However, at a given altitude, XCr values higher than ~55 are generally observed in the more concentrated ores (scattered, antinodular or massive samples) rather than in the more disseminated ones (rare or very scattered chromite samples).

In detail, Cr and Al, which typically substitute for each other in spinel, show an unexpected decoupling at some levels. Although their concentrations are anti-correlated at the scale of the whole stratiform chromitite, they show a parallel decreasing trend within the intermediate breccias system (1030-1034 m) as well as above the altitude 1058 m (correlated to the TiO_2 content and negatively correlated to YFe^{3+}). Otherwise, in between the three highest breccias (1049-1053 m), the Cr_2O_3 content shows two successive increasing and decreasing trends within a few metres while Al_2O_3 continuously increases on the same interval. XMg shares basically the same evolution as XCr and is particularly well-correlated to the Cr_2O_3 content, while oppositely YFe^{3+} is negatively correlated to XMg (Fig. 7a). The vertical evolution of the TiO_2 content is decoupled from the other chemical species/atomic ratios and shows, with few local exceptions, a global and relatively monotonous increase from about 0.30 wt% at the base of the stratiform chromitite to 0.50 wt% to its top (Fig. 7a). The few local exceptions occur generally at altitudes where magmatic breccias were observed.

351

352 *4.3. Silicate matrix*

353 *4.3.1. Olivine*

354 The olivine matrix shows marked variations in composition with Fo (100 × Mg/(Mg +
355 Fe_{total}) atomic ratio) = 90.4-95.2, NiO = 0.34 to 0.64 wt%, and CaO ranging from detection
356 limit to 0.16 wt% (averaged per thin section). Vertical variations of both the Fo and the NiO
357 content are closely correlated to the XCr, especially to the Cr_2O_3 content, and to the XMg of
358 chromite (Fig. 7a-c). We observe scattered values in Fo and NiO at the base of the stratiform
359 chromitite, overlain by common and successive (1) decrease in between the two intermediate
360 breccias, (2) increase to highest breccias (with a much higher variability at the altitude 1040
361 m) and (3) decrease within the uppermost part of the ore body. MnO content is conversely
362 anti-correlated to those chemical species/ratios (not shown). High CaO values of the olivine
363 matrix (i.e. higher than 0.05 wt%) are restricted to the base of the stratiform chromitite,
364 particularly around the lowest breccia at the altitude 1020 m (Fig. 7b). Beyond these global
365 trends at the scale of the stratiform chromitite, alternations of increases and decreases in a
366 given element or elemental ratio can be observed at a finest scale, especially from the highest
367 breccias and above.

368

369 *4.3.2. Clinopyroxene*

370 Clinopyroxene, the second most abundant mineral phase after olivine in the matrix,
371 shows XMg (100 × Mg/(Mg + Fe^{2+}) atomic ratio, average per thin section) varying between
372 91.1 and 94.9, and Al_2O_3 = 1.8-4.4 wt%, Cr_2O_3 = 1.1-1.5 wt, TiO_2 = 0.15-0.38 wt% and Na_2O
373 = 0.22-0.58 wt%. The XMg of clinopyroxene is correlated to Fo of olivine (and XMg of
374 chromite) (Fig. 7c). While most difficult to decipher, the vertical evolution of both Al_2O_3 and
375 TiO_2 contents of clinopyroxene, as well as of Na_2O (not shown), is negatively correlated to

376 the one of XMg. The few analysed hybrid diopsides (i.e. hybrid in composition between
377 igneous clinopyroxene and pure hydrothermal diopsides; Rospabé et al., 2017) show higher
378 XMg (94.3-97.0) and SiO_2 content (53.8-55.0 wt% instead of 51.8-53.6 wt%) coupled with
379 lower Al_2O_3 (0.47-1.4 wt%), TiO_2 (0.03-0.16 wt%) and Na_2O (<0.23 wt%) contents than in
380 clinopyroxene whose composition fits with an igneous origin.
381
382 *4.3.3. Orthopyroxene*
383 The few orthopyroxene occurrences in the matrix are enstatites, with XMg (100 ×
384 Mg/(Mg + Fe^{2+}) atomic ratio) = 92.2-94.0, Al_2O_3 = 1.33-1.38 wt%, CaO = 0.62-1.48 wt% and
385 TiO_2 = 0.13-0.15 wt% (Table 1 and Supplementary Material).
386
387 *4.3.4. Amphibole*
388 Excepting for one sample (06OM04-10, 1036 m), the matrix contains amphibole only
389 above the higher breccias system in the uppermost part of the stratiform chromitite ore body.
390 Amphibole is mostly pargasitic to edenitic hornblende. The variation ranges of XMg (100 ×
391 Mg/(Mg + Fe^{2+}) atomic ratio) and XNa (100 × Na/(Na + K) atomic ratio) are 89.6-92.4 and
392 91.7-98.2 respectively (Na_2O = 2.5-3.1 wt%; K_2O = 0.08-0.40 wt%). The TiO_2 content of
393 amphibole varies from 0.30 to 1.8 wt%. Similarly to what was described for the Al_2O_3 content
394 of chromite and for other chemical species in olivine and clinopyroxene (Fig. 7a-c),
395 amphibole composition evolves differently below and above the altitude 1058 m. Below this
396 level, XMg decreases from 92.4 to 90.1 and XNa and TiO_2 increase from 96.8 to 91.7 and
397 from 1.5 to 1.8 wt% respectively. Above this level, the reverse trend is observed, XMg, XNa
398 and TiO_2 evolving to 90.9, 98.2 and 0.30 wt% respectively.
399
400 *4.3.5. Garnet*

Garnet observed at the same levels where the amphibole occurs is mostly grossular (sum of oxides ranging from 97.8 to 100.2 wt%), with SiO_2 = 36.0-39.6 wt%, CaO = 36.9-38.2 wt% and Al_2O_3 = 21.1-22.6 wt%. The Cr_2O_3 and TiO_2 contents are comprised between 0.09 and 1.36 wt%, and 0.03 and 0.15 wt% respectively (Table 1 and Supplementary Material).

4.4. Chemical profiles across samples: chromite-matrix composition co-variations

In order to better describe the mm- to cm-scale composition co-variations in chromite and olivine (and clinopyroxene when present), we performed chemical profiles across four samples 06OM04-3B2 (alt. 1021.5 m), -5D (1030.5 m), -12E1 (1040.3 m) and 04OM31E (collected apart from the cross-section, very near the base of the stratiform chromitite) (Fig. 8).

The samples selected display mm- to cm-scale extremely variable chromite and olivine modal contents, covering the entire variation range described previously (from rare chromite in dunite to massive chromitite). Despite differences in terms of absolute chemical compositions from one sample to another, these samples share common relationships between chemical and modal variations. Higher amounts of chromite are perfectly correlated to higher XMg of chromite and Fo of olivine: Fo reaches values of about 90.5 in chromite-bearing dunites (rare disseminated chromite) to 94.5 in antinodular to massive chromitites. The NiO content of olivine, despite a high scatter, is correlated to the Fo. The TiO_2 content of chromite displays a small-scale high dispersion; however, it seems that highest values are generally observed in antinodular to massive ore portions.

The main difference with the chemical variations at the scale of the whole stratiform ore body resides in the distribution of Cr, ^{IV}Al and Fe^{3+} in chromite. In samples - or parts of thin sections - with the highest amount of chromite (scattered, antinodular and massive), Cr

and Al are negatively correlated (Fig. 8b-c-d), with the highest Cr values (up to 1.06 apfu) observed where the amount of chromite is high. Oppositely, in portions containing disseminated chromites (rare or very scattered), Cr and Al increase or decrease concomitantly while Fe^{3+} is negatively correlated to those two chemical species (Fig. 8a-b). In these cases, Cr and Al generally decrease together and Fe^{3+} increases as the sample becomes more dunitic.

The thin section of sample 06OM04-12E1 shows interstitial clinopyroxene, restricted to the decreasing peak of the amount of chromite and above, within the upper massive interval (Fig. 8d). Within this interval, we observed the increase of XMg (from 94.0 to up to 99) associated to the decrease of Al_2O_3 (from 2.6 to 1.4 wt%), TiO_2 (from 0.29 to 0.20 wt%) and Na_2O (from 0.38 to 0.22 wt%) contents of clinopyroxene.

In a different view, Figure 9 shows that in the four samples (06OM04-3B2, -5D, -12E1 and 04OM31E), the evolution of Fo of olivine and of XMg, XCr, YFe^{3+} and TiO_2 of chromite follows the chromite abundance. Systematically Fo and XMg increase and YFe^{3+} decreases when variations in the chromite modal content ranges from 0 to 30-40% chromite. Above 40%, there is no more evolution of these chemical ratios which seem to be buffered to values of about 93.5, 65 and 4.5 respectively. XCr is constant around 53 in the two samples 06OM04-5D and 04OM31E whatever the chromite modal abundance, and tends to this value in the two other samples when the chromite abundance becomes lower than 40% (i.e. steady values near 49 and 57 in 06OM04-3B2 and -12E1 respectively above 40% of chromite). The TiO_2 content does not show marked variation from below to above 40% of chromite, and appears not affected by the variation of the chromite modal content excepting a very slight and constant increase from scarce to massive ores.

4.5. Silicate inclusions

4.5.1. Orthopyroxene

Orthopyroxene in inclusion in chromite is enstatite, with a similar XMg (92.5-94.5), slightly higher Cr_2O_3 (0.60-1.2 wt%) and lower Al_2O_3 (0.41-1.3 wt%), CaO (0.21-0.83 wt%) and TiO_2 (0.05-0.11 wt%) contents than those of the few orthopyroxene crystals observed in interstitial position and associated to the other matrix minerals. Higher XMg values are observed along the interval 1040-1050 m (Fig. 7d), together with high XCr and XMg of chromite (Fig. 7a) and high Fo of olivine and XMg of clinopyroxene (Fig. 7b-c). In the same way, Al_2O_3 and TiO_2 contents increase together from 1026 to 1036 m, decrease to about 1050 m, then globally re-increase to the top of the stratiform chromitite with a clear disturbance around the altitude 1058 m (Fig. 7d). These variations largely mimic the ones observed for Al_2O_3 of host chromites and for Al_2O_3 and TiO_2 contents of matrix clinopyroxene.

4.5.2. Clinopyroxene

The less common inclusions of clinopyroxene exhibit variable XMg (93.0-97.3) and Na_2O content (0.54-1.3 wt%), both higher than those of the clinopyroxene in the matrix. These inclusions show more restricted Al_2O_3 (2.4-2.6 wt%), Cr_2O_3 (1.3-1.6 wt%) and TiO_2 (0.20-0.36 wt%) compositional ranges (averaged per thin section). Only one inclusion of diopside of likely hydrothermal origin (cf. Python et al., 2007; Rospabé et al., 2017) was found. Its XMg and Al_2O_3, Cr_2O_3, TiO_2 and Na_2O contents values are 96.0, 1.0 wt%, 0.73 wt%, 0.22 wt% and 0.20 wt% respectively.

4.5.3. Amphibole

Amphiboles occurring as inclusions in chromites are pargasites/pargasitic hornblendes, for more than 60% of them, or magnesio-hastingsites/magnesio-hastingsitic hornblendes, for more than 30% of them. The XMg and TiO_2 content values, averaged for each sample, are much variable (88.8-93.3) and higher (1.8-2.8 wt%), respectively, compared

476 to those of amphiboles from the matrix. Within each sample, the variability from an
477 amphibole inclusion to another is much higher than concerning amphibole in the matrix (Fig.
478 7e). Their Na_2O content ranges from 2.9 to 4.1 wt%, while their K_2O content is lower than
479 0.10 wt%, making their XNa to be restricted to very high values (98.2-99.3). The vertical
480 evolution of XMg and Al_2O_3 values basically follows the same tendency observed in
481 orthopyroxene inclusions. However, the distribution of the TiO_2 content is much scattered,
482 with a certain increase from lower to higher values from the base to the top of the stratiform
483 chromitite (Fig. 7e).
484
485 *4.5.4. Mica*
486 Micas, absent in the matrix and observed solely as inclusions, have compositions
487 evolving from phlogopite to aspidolite (Na-rich phlogopite) end-members. Their averaged
488 XMg and Cr_2O_3 and (high) TiO_2 contents range from 93.7 to 96.2, from 1.9 to 3.0 wt% and
489 from 2.6 to 4.3 wt% respectively. Micas are also characterized by high Na_2O (3.1-5.6 wt%)
490 and moderate K_2O (0.61-3.8 wt%) contents (Na_2O + K_2O = 6.1-7.0 wt%), the XNa varying
491 from 55.0 to 93.2 (averaged per thin section). Vertically along the stratiform chromitite, mica
492 composition follows the same evolution observed in other minerals, with high XMg values
493 along the interval of 1040-1050 m and a common evolution of their Al_2O_3 and TiO_2 contents
494 (not shown). The XNa values lower than 90 (enrichment in K_2O relative to Na_2O) are
495 observed at the base of the ore body, in between the lowest and the intermediate breccias, as
496 well as along its uppermost part within and above the higher breccias system (Fig. 7f). These
497 lower XNa values result either, in a given sample, from compositions evolving continuously
498 from Na-rich to K-rich end-members (e.g. sample 06OM04-5C2 (1030 m) with Na_2O = 0.34-
499 6.3 wt%, K_2O = 0.32-6.9 wt% and XNa = 7.0-96.8), or from the average of values from two
500 distinct populations within a single sample (e.g. sample 06OM04-4 (1026 m) with Na_2O =

501 1.3-2.7 wt% and K_2O = 2.7-7.2 wt% in the first population, and Na_2O =5.9-6.9 wt% and K_2O
502 = 0.17-0.60 wt% in the second population, giving XNa = 27.9-42.7 and 93.7-98.3
503 respectively).
504
505 *4.5.5. Other inclusions*
506 Similarly to what is observed in the matrix, the few garnet inclusions in chromite are
507 grossular. We identified also two nepheline inclusions that are sodic (K-poor) and Si-rich,
508 with Na_2O, SiO_2 and Al_2O_3 averaged contents of 18.7 wt%, 49.3 wt% and 30.6 wt%,
509 respectively (K_2O = 0.14 wt%) (Supplementary Material).
510 A silica-rich inclusion identified in the sample 06OM04-17 has high SiO_2 (76.0 wt),
511 Al_2O_3 (17.7 wt%) and Na_2O (8.6 wt%) concentrations, and a minor FeO content (0.32 wt%).
512 While the nature of this very minor phase if quite enigmatic, its composition fits with a
513 submicronic-scale mixing between ~80% albite and ~20% quartz. It might be a microperthite.
514
515 **5. Discussion**
516 *5.1. Structure and petrology of the stratiform ore body*
517 The Maqsad area is characterized by a high abundance of podiform chromitites
518 (Borisova et al., 2012; Ceuleneer and Nicolas, 1985; Leblanc and Ceuleneer, 1991; Rollinson
519 and Adetunji, 2013; Rollinson et al., 2018; Zagrtdenov et al., 2018), defining one of the most
520 important chromitiferous district in the Oman ophiolite. The ore deposits occurring within the
521 dunitic mantle-crust transition zone at the top of the Maqsad diapir, including the studied
522 stratiform chromitite ore body, developed during the last stage of the upwelling of the
523 asthenospheric mantle diapir. Accordingly, they escaped solid-state deformation related to the
524 spreading ridge activity and off-axis transposition. The layered structure of the stratiform
525 chromitite, the preservation of delicate igneous texture, including graded bedding, the absence

526 of any sign of solid-state deformation (Figs. 3 and 4), and the entrapment of silicate inclusions
527 (Fig. 5), evoke a pile of layered cumulates whose crystallization was synchronous with the
528 one of the overlying gabbroic lower crust.

529 The stratiform ore body consists of interlayered levels of scattered chromite in dunites
530 and of more concentrated levels, mostly with antinodular textures but hosting layers of
531 massive chromitites a few cm- to 3 m-thick (Figs. 2c and 3). Another significant feature is the
532 presence of levels of magmatic breccias, a few tens of cm in thickness at most, made of
533 angular wehrlitic fragments (i.e. dunites displaying a higher clinopyroxene content than
534 average in this part of the DTZ) in the chromitite, all together embedded in the olivine matrix
535 (Fig. 3h-i). They most likely witness successive melt injection events, potentially with
536 increased melt/mush ratios, during the formation of the stratiform ore body. Other related
537 melt segregation and injection textures reflecting the former dynamic environment were
538 frozen at some levels (Fig. 3f-g). Chromite-rich layers I, II and IV were found at the same
539 levels where were described the lower, intermediate and higher brecciated systems
540 respectively (Fig. 2). However, the fact that the two layers III and V seem to be unrelated to
541 these features allows concluding that breccias and related melt injections do not solely control
542 the local concentration of Cr.

543 The three-dimensional structure of the stratiform chromitite is difficult to assess due to
544 erosion; however, its lateral extension apparently did not exceed a few hundred metres
545 regarding the significant decrease of the chromite modal content in surrounding outcrops.
546 Originally, as suggested by its shape before mining (Fig. 3a), it was probably formed as a
547 circular lens bordered to the southwest by a high temperature N130-oriented normal fault.
548 This fault presently makes the contact between, to the SW, layered troctolites that originally
549 formed higher up in the section, and, to the NE, dunites from the DTZ that host the stratiform
550 chromitite.

551 The mineral distribution confers to the stratiform chromitite a major and remarkable
552 contrast between (1) minerals constituting the matrix between chromite grains, mostly
553 anhydrous (olivine, clinopyroxene) except for its upper part (amphibole, garnet), and (2)
554 minerals of the chromite-hosted inclusions which are, as a rule, hydrous or anhydrous silicates
555 (mostly amphibole, orthopyroxene and mica) witnessing the high silica and water contents in
556 their parental melt/fluid. The origin of the silicate inclusions enclosed in chromite grains from
557 Oman ophiolite chromitites were interpreted either as *in situ* crystallization products from
558 trapped melt inclusions (e.g. Schiano et al., 1997; Rollinson et al., 2018), or as solid phases
559 already crystallized in the parent magma and that were subsequently trapped when chromite
560 formed (e.g. Borisova et al., 2012). The fact that the surrounding Maqsad DTZ dunites
561 contain numerous mineral impregnations that are actually fractional crystallization products
562 from percolating melts (e.g. Boudier and Nicolas, 1995; Koga et al., 2001; Abily and
563 Ceuleneer, 2013), including widespread orthopyroxene and amphibole in the upper level of
564 the DTZ (Rospabé et al., 2017), suggests a common origin and supports the view that most
565 silicate inclusions in chromite were already crystallized prior to their entrapment. Otherwise,
566 it is worth noting that the silicate inclusions in the stratiform chromitite become more
567 abundant approaching the intermediate and higher magmatic breccias systems (Fig. 2). This
568 observation suggests that the same dynamic event leading to the breccias formation triggered
569 the sudden crystallization of silicate crystals that would eventually be entrapped by chromite.
570
571 *5.2. Chemistry of the stratiform ore body*
572 Averaged XCr values of chromite from the stratiform ore body are relatively moderate
573 (49.0-59.9), similar to those of the disseminated chromite from the surrounding DTZ and
574 contrasting with those of other ore bodies and their host dunites elsewhere in Oman,
575 especially in the northern massifs of the ophiolite where XCr can reach much higher values

576 (Ahmed and Arai, 2002; Augé, 1987; Miura et al., 2014; Rollinson, 2008; Rollinson and
577 Adetunji, 2015). Evenly, the TiO_2 content of the stratiform chromite is typically high (0.25-
578 0.54 wt%), a characteristic shared by most chromitites and scattered chromites in dunites
579 from the Maqsad area and contrasting with widespread lower values observed in almost all
580 other massifs of the Oman ophiolite. This is a major evidence for the MORB kindred of the
581 parent melt of the various igneous products issued from the Maqsad diapir (Clénet et al.,
582 2010; Python et al., 2008), including chromitites (Borisova et al., 2012; Leblanc and
583 Ceuleneer, 1991; Zagrtdenov et al., 2018).

584 Mineral chemical compositions show significant variations at different scales, both
585 locally at a single altitude and at the scale of the whole stratiform chromitite (Figs. 6 and 7).
586 At the local scale, variations mainly concern XMg and YFe^{3+} of chromite and Fo and the NiO
587 content of olivine, and are clearly related to thin section scale variations in the modal
588 proportion of chromite and olivine (Fig. 8). This is observed for intervals with a chromite
589 modal content ranging from 0 to 30-40%. Above 40% of chromite, the chemical compositions
590 do not evolve anymore, suggesting a buffering process around a composition possibly in
591 equilibrium with the chromite parent melt (Fig. 9).

592 In contrast, chemical variations vertically along the stratiform ore body define
593 complex trends of higher amplitude than locally, mostly concerning the XCr of chromite and
594 in a lesser extent the Fo, NiO and CaO contents of olivine as well as the clinopyroxene
595 composition (Fig. 7a-c). This is reminiscent of the trends observed globally all across the
596 DTZ (Abily and Ceuleneer, 2013; Rospabé et al., 2018, 2019). Parallel trends are observed in
597 the composition of silicate inclusions in chromite, as in the TiO_2 content of amphibole and
598 alkalis of mica (Fig. 7d-f). The high amplitude of these variations cannot have solely resulted
599 from sub-solidus re-equilibration. *Interestingly, these large-scale trends do not mirror at all*
600 *the variations in modal composition of the ore but correlate to the presence of the three*

magmatic breccia systems (i.e. we observe continuous trends bounded by the three levels where brecciated levels are concentrated).

Accordingly, this suggests that the current chemical characteristics along the stratiform chromitite result from multi-scale processes: the development of high temperature, magmatic breccias have extensively controlled the large scale chemical evolution of the whole chromitite ore body, while the chromite mode and subsolidus chemical re-equilibration affected the small, mm to cm-scale chemical variations.

More generally, the olivine matrix from the stratiform chromitite displays Fo and NiO content significantly higher than in nearby dunites from the DTZ and in mantle harzburgites from the Sumail massif, reaching values up to 95.3 and 0.63 wt% respectively (Fig. 10a). Even higher values were reported for mantle chromitites from the north of the Oman ophiolite (Augé, 1987; Miura et al., 2014; Rollinson, 2008, 2019) (Fig. 10b). In the Sumail massif, all podiform chromitites share the same feature, their olivine matrix falling in the same chemical variation range whatever they outcrop within the DTZ or the mantle section. Furthermore, a chromitite dike from the Maqsad DTZ, located few hundred metres to the northeast of and at a higher structural level than the present stratiform ore body, displays higher olivine Fo values in olivine-plagioclase nucleus around which chromite nodules grown than in the olivine matrix surrounding nodules (Zagrtdenov et al., 2018). Taken together, these two observations allow us suggesting that Mg-Fe^{2+} post-magmatic subsolidus exchanges between chromite and olivine (e.g. Cameron, 1975; Fabriès, 1979; Grieco et al., 2018; Lehmann, 1983; O'Neill and Wall, 1987) cannot solely explain such high Fo values associated to high NiO content along the stratiform chromitite: (1) first, the contrast between DTZ and mantle chromitites from the Sumail massif on one hand and mantle chromitites from the northern massifs on the other hand matches with the two main magmatic series identified along the Oman ophiolite. These series were highlighted following the nature of cumulates frozen in the mantle section (i.e.

626 MORB mainly, but not only, in the SW of the Oman ophiolite, more widespread depleted
627 calc-alkaline in the central and northern massifs; Python and Ceuleneer, 2003; Python et al.,
628 2008); (2) then in the case of the other chromitite dike (Zagrtdenov et al., 2018), later re-
629 equilibration should have affected equally olivine in nucleus and olivine in the matrix, which
630 is not the case. However, it might strongly depend on the scale we are investigating these
631 chemical variations.

632 The compositions of coexisting olivine and chromite (Figs. 7 and 8) suggest
633 subsolidus re-equilibration at 800 to 900°C, as commonly observed in metamorphosed
634 peridotites (Evans and Frost, 1975). In such rocks, the partitioning of Mg and Fe^{2+} depend on
635 the volume ratio of olivine to chromite as well as on temperature (e.g., Arai, 1980).
636 Interestingly, other studies report on a negative (and not positive as in our case) correlation
637 between Fo of olivine and XMg of chromite (e.g. Bussolesi et al., 2019). These authors
638 interpret this correlation in terms of solid-state exchange of Mg and Fe between olivine
639 (incorporation of Mg) and chromite (incorporation of Fe) grains. In our case this process
640 alone doesn't fit simple mass balance consideration as the correlation between XMg and Fo is
641 also associated to variations in the NiO content of olivine and in the XCr, YFe^{3+}, and
642 sometimes TiO_2 of chromite. An avenue of explanation might be to evoke a percolating
643 interstitial melt (i.e. an open system), re-equilibration being likely triggered by such an
644 interstitial melt that makes diffusional processes more efficient. The equilibration is limited in
645 space, possibly in a few cm^3, and the mass balance for Mg and Fe have been maintained in the
646 restricted area.

647 At a much larger scale, the variations observed over up to 10 m vertically are likewise
648 correlated to other chemical indexes such as XCr (Fig. 7), and are not correlated to the ore
649 concentration as was stressed before (Fig. 2). The chemical composition thus better result
650 from the primary processes that originated the stratiform chromitite, including the

651 development of the magmatic breccias, rather than from secondary processes.

652

653 *5.3. Tentative scenario for the formation of the stratiform ore body*

654 Since decades, several mechanisms were proposed to account for the formation of
655 chromitite ore bodies: mixing between contrasted magmas, addition of SiO_2 and/or H_2O,
656 change in the pressure among others (e.g. Irvine, 1975, 1977a, 1977b; Latypov et al., 2018;
657 Lipin, 1993; Matveev and Ballhaus, 2002; Mondal and Mathez, 2007; Naldrett et al., 2012;
658 Spandler et al., 2005). One of the most popular models is the one of Irvine (1975, 1977a),
659 which proposed that massive crystallization of chromite is triggered by the mixing between a
660 basaltic melt saturated in chromite and a more silicic melt (the same melt at a more evolved
661 stage, or felsic contamination by assimilation of crustal rocks surrounding the magma
662 reservoir). More generally, it was also proposed that the nucleation of 'crustal-like' minerals
663 associated to the massive chromite crystallization may result from the hybridization between
664 the basaltic fraction and a siliceous volatile- and Na-rich fluid or melt fraction (e.g. Johan et
665 al., 1983, 2017; McElduff and Stumpfl, 1991; Spandler et al., 2005; Talkington et al., 1984).
666 In other studies, it was shown that this mixing process cannot account for the formation of
667 some chromitites, especially in the Bushveld Complex (e.g. Mondal and Mathez, 2007;
668 Naldrett et al., 2012). It is probable that a single model cannot consensually explain the
669 formation of all chromitites worldwide, in old intracontinental intrusions or in ophiolites, but
670 that different processes, working alone or together, may lead to the formation of a given ore
671 body.

672 In the Maqsad area, we evidenced witnesses of the involvement of such hybrid melts
673 or fluids. The partial melting within the Maqsad diapir produced 'dry' (i.e. water poor)
674 MORB, evidenced by the petrology (nature, crystallization sequences) and geochemistry of
675 troctolite and ol-gabbro that crop out in the harzburgitic mantle sequence (Benoit et al., 1996;

676 Ceuleneer et al., 1996; Python et al., 2003). However, the widespread occurrence of
677 orthopyroxene, amphibole, diopside and garnet, interstitially between olivine grains in the
678 DTZ dunites (i.e. thus at a higher structural level) attests to the genesis of hydrous melts at the
679 mantle-crust transition zone (Rospabé et al., 2017; 2018). We proposed that it resulted from
680 the hybridization between the uprising MORB and a hydrated component coming from above,
681 probably seawater in origin and potentially trondhjemitic in nature following the hydrous
682 melting of the country rocks (see also Amri et al., 1996; Benoit et al., 1999; Koepke et al.,
683 2005, 2014; Nonnotte et al., 2005 concerning the hydrous re-melting of the shallow mantle
684 and deep crust beneath oceanic spreading centres). The similar minerals, interstitially in
685 dunites and in inclusions in both disseminated chromites in dunites and more concentrated
686 chromitites, allowed concluding that the hybrid melt was strongly involved in the formation
687 of both dunites and chromitites from the Maqsad DTZ following melt- or magma-fluids-
688 harzburgite reactions (Rospabé et al., 2017, 2018). Returning to the stratiform chromitite, it
689 allows us to favour the hypothesis of the mixing, or hybridization, between contrasted melts
690 and/or fluids at its origin.

691 The relationship between (1) the location of brecciated levels, (2) the vertical chemical
692 evolution of all mineral phases along the stratiform chromitite, and (3) the higher abundance
693 of orthopyroxene, amphibole and micas included in chromite grains, supports that melt or
694 magma injections strongly influenced the composition of the parent melt from which
695 crystallized the ore body. The existence of such injections is witnessed by the several levels of
696 breccia interlayered with the dunites and chromitites. Especially, the decoupling between the
697 zigzag variation pattern in XCr, and the smooth increase of the TiO_2 content of chromite,
698 from the base to the top of the ore body (Fig. 7a), cannot result solely from fractional
699 crystallization from a single melt batch. It probably reflects the involvement of several melt
700 injections and of melt fractions of contrasted composition. Additionally, it was shown in the

701 Maqsad area that fault zones developed early, during oceanic spreading and crystallization of
702 the crust, and were probably the main vectors for the introduction of the hydrated component
703 in the lower oceanic crust and at Moho level (Abily et al., 2011; Rospabé et al., 2019). In this
704 way, magmatic breccias we observe within the stratiform chromitite may represent the
705 nucleation state of such syn-magmatic faults, developed within a still unconsolidated mush
706 and responsible of fluids and/or melt pulses that hybridized with magmatic mush containing
707 interstitial MORB. The hybridization from brecciated levels may have thus been responsible
708 for:

709 - The precipitation of Ti-rich chromites that entrapped mainly orthopyroxene-
710 amphibole-mica and high XCr chromites, which were all microcrystals in suspension in the
711 former hydrated Si- and Na-rich melt or fluid (e.g. Matveev and Ballhaus, 2002);

712 - The higher amount of orthopyroxene, amphibole and mica in inclusion in chromite at
713 the same levels than the breccias (Fig. 2);

714 - The higher XCr of chromite and Fo and NiO content of olivine toward the higher
715 breccias system (Fig. 7), buffered to high values due to a particularly strong involvement of
716 the hydrated component at this specific level, probably with a higher supply of the hydrated
717 melt (possibly saturated with a fluid);

718 - The local correlation between Cr and Al near breccias, negatively correlated to the
719 Fe^{3+} (Figs. 6 and 7), being the imprint of a disturbance of the Cr-Al substitution process by
720 the involvement of such hydrated melt/fluids at these levels;

721 - The widespread occurrence of clinopyroxene and the total absence of plagioclase
722 interstitially between olivine grains in the dunites hosting the stratiform chromitite (Fig. 2;
723 wehrlitic dunites in Figs. 3h and 4h). It probably crystallized from the newly hybrid MORB,
724 more evolved (continuous increase of the TiO_2 content of chromite, Fig. 7) and hydrated
725 (appearance of interstitial amphibole and garnet in the upper part of the stratiform chromitite;

Fig. 2) upsection, after the solely crystallization and concentration of chromite.

However, while the hybridization of the MORB with the hydrated Si- and Na-rich melt/fluid along the magmatic breccias is responsible for the distribution of the silicate inclusions and of the whole chemical structuration of the stratiform chromitite (e.g. richness in Cr), the hybridization influenced only partly the ore concentration (i.e. chromite modal content). It is explained here by the fact that the chromite-rich layers I, II and IV only are correlated to the presence the magmatic breccias, whereas the layers III and especially V (that is the most massive, 3 m in thickness; Figs. 2c and 3) show no evident influence of the magmatic breccias and calls for another explanation. Although as a working hypothesis, the decoupling between the chromite modal concentration and its Cr concentration may be accounted by the small-scale highly contrasted saturation in chromite of the former MORB before its hybridization. It was shown that highly variable fractions of melts percolated through the Maqsad DTZ (Rospabé et al., 2018), and that decoupling may thus also reflect the locally variable advancement of the hybridization process (or with which proportions of each of the two contrasted melt/fluid the hybridization operated). In this context, it is likely that podiform chromitites form early during the development of the mantle-crust transition zone as a companion product of the dunites' formation.

Conclusion

This paper illustrates the usefulness of studies combining accurate field descriptions and dense sampling of chromite ore bodies. The high quantity of samples reveals the variability in composition of the mineral composition while the origin of this variability can be understood if and only if each sample is positioned in its geographical and structural context.

In the case of the Maqsad stratiform chromitite, our study has established that no

relationship exists between the distribution of the layers of massive ore (i.e. chromite modal content) and the variation patterns of the chemical composition of the ore (i.e. richness in Cr) and of associated silicate minerals. However, these patterns are consistent with the distribution of magmatic breccias, and hence of melt injection in crystallizing cumulates. Accordingly, different processes condition the variations in ore concentration on one hand and in ore composition on the other hand.

The major contrast between the nature of the silicate minerals making the ore matrix and of the silicates entrapped within the chromite grains confirms that hybridization between a primitive basaltic melt (of MORB-type in the case of this particular ore body) and a hydrous silica-rich melt of possible hydrothermal origin primarily conditions the formation of chromite ore bodies as well as of the dunitic matrix at the mantle-oceanic crust transition zone.

Acknowledgments

M.R. and G.C. are very indebted to F. de Parseval for thin sections preparation and to Ph. de Parseval for assistance during microprobe data acquisition. We are extremely grateful to our colleagues from the Public Authority of Mining, M. Al Araimi, M. Almusharrafi, M. Al Batashi, A. Al-Rajhi and H. Al Azri, for their constant support and hospitality during field work in Oman. Constructive comments and suggestions from A. Kapsiotis, E. Mathez and the editor A. Kerr greatly helped to improve the manuscript. This work has benefited from a financial support provided by the French CNRS (Centre National de la Recherche Scientifique) through the TELLUS/SYSTER program of INSU (Institut National des Sciences de l'Univers).

Figure captions

Figure 1: a) General map of the different massifs constituting the Oman ophiolite. b) Geological map of the studied Maqsad area in the Sumail massif, modified after Zagrtdenov et al. (2018) (enlargement of the square in Figure 1a). The red star indicates the stratiform chromitite investigated in this study, and located within the dunitic mantle-crust transition zone. White stars are other chromitite ore bodies occurring in the Maqsad area.

Figure 2: Petrological log of the cross-section sampled along the stratiform chromitite ore body. Collected samples (labels are reported to the right of the petrological log) are classified in five main lithological groups depending on their chromite modal content, from rare (dunites containing few percent) to very scattered, scattered, antinodular and massive. The five layers that show a particularly high chromite modal content are annotated from I, the lowest chromite-rich level, to V, the highest one. Magmatic breccias are reported at the altitude they were described on the field (light blue lines). The six main brecciated levels are described as the lower breccia (1020 m), the intermediate breccias system (two breccias at altitudes 1030 and 1034 m), and the upper breccia systems (three breccias in between 1046 and 1052 m). The table in the middle reports the presence/absence of each identified silicate phase in the matrix (mainly olivine and clinopyroxene) or occurring as inclusion in chromite (mainly orthopyroxene, amphibole and mica). The diagram to the right represents the relative abundance of inclusions, from 0 to 8, based on thin sections observations using optical microscope. The value 1 corresponds to samples containing only rare chromite grains that enclose one or two silicate inclusions at most; the value 8 was attributed to samples in which almost all chromite grains contain several (more than 10 in some cases) silicate inclusions. Inclusions were observed in all the samples from the studied set, explaining that no one was classified as 0 (absence of inclusion). Abbreviations as following: am: amphibole; cpx: clinopyroxene; di: hybrid diopside; gt: garnet; mi: mica; ne: nepheline; ol: olivine; opx:

orthopyroxene.

Figure 3: Field photographs along the stratiform chromitite. a and b) View of the stratiform chromitite before (a: 2006) and after (b: 2016) its exploitation by mining companies. c) Massive chromitite, about 3 m thick, near the top of the stratiform ore body. d) Layered gradual variations ("graded beddings") of the relative modal abundance of chromite and of olivine. e) Sharp transition from layered scattered to antinodular texture to massive chromitite. f and g) Migration (f) and injection (g) textures within the olivine-rich matrix. h and i) Magmatic breccias composed of angular dunitic fragments included in surrounding chromitite.

Figure 4: Insights of increasing abundance of chromite in thin sections (natural light) from a) scarce (06OM04-1) to b) very scattered (06OM04-2A), c) scattered to antinodular (06OM04-3C1), and d) antinodular (to the left) to massive (to the right) (06OM04-6B2). e) Small-scale (mm to cm) variation of chromite mode within single samples (to the left 06OM04-5A, to the right 06OM04-5B). f) Brecciated sample 06OM04-6B1 composed of chromitite and clinopyroxene-bearing dunite fragments. g) Olivine matrix (two grains) in an antinodular to massive chromitite sample (06OM04-21C). h) Antinodular texture formed by chromite and oikocrystic clinopyroxene (06OM04-19(1)). Numerous inclusions are observed within chromite grains.

Figure 5: Photomicrographs of a few examples of silicate inclusions in samples from the stratiform chromitite. (a and b) The two first pictures show that silicate inclusions are sometimes organized as coronas within the chromite grain (circled by the white arrows), surrounding a central inclusion (06OM04-10 and -12B2C). (c) Enlargement of (b) showing

826 the central amph-opx-mica polymineralic inclusion. (d) Polymineralic inclusion made of the
827 amphibole-mica-nepheline assemblage (06OM04-03A). (e) Large (> 100 µm) and well-
828 preserved inclusion of grossular garnet in transmitted and crossed-nicols lights to the left
829 (06OM04-26). The pictures in transmitted light to the right allow appreciate the isotropic
830 character of the garnet. (f and g) Another example of a corona of inclusions (f). The inclusion
831 to the top right (g), possibly a microperthite, has a silica-rich composition which fits with a
832 mixture made of albite and quartz (06OM04-17). Abbreviations are as follows: amph,
833 amphibole; gt, grossular garnet; ne, nepheline; opx, orthopyroxene.
834
835 **Figure 6:** Chromite chemical composition from the stratiform chromitite, illustrated in an
836 enlargement of the Cr-Al axis from the ternary Al-Cr-Fe(III) diagram (top) and in the
837 variation of XCr and of the TiO_2 content as a function of XMg and XCr respectively
838 (bottom). XCr = 100 × Cr/(Cr + Al) atomic ratio; XMg = 100 × Mg/(Mg + Fe^{2+}) atomic ratio.
839 The colours of the dots represent the chromite modal content in each analysed sample, as rare
840 in light green, very scattered in green, scattered in orange, antinodular in red and massive in
841 black.
842
843 **Figure 7:** Vertical evolution of the mineral chemical composition along the studied stratiform
844 chromitite, plotted as a function of the absolute altitude. a) the XCr (100 × Cr/(Cr + Al)
845 atomic ratio), the Cr_2O_3 and Al_2O_3 contents, the XMg (100 × Mg/(Mg + Fe^{2+}) atomic ratio),
846 the YFe^{3+} (100 × Fe^{3+}/(Cr + Al + Fe^{3+}) atomic ratio) and the TiO_2 content of chromite, in b)
847 the Fo (100 × Mg/(Mg + Fe_{total}) atomic ratio) and the NiO and CaO contents of olivine matrix,
848 in c) the XMg (100 × Mg/(Mg + Fe^{2+}) atomic ratio) and the Al_2O_3 and TiO_2 contents of
849 clinopyroxene matrix, in d) the XMg (100 × Mg/(Mg + Fe^{2+}) atomic ratio) and the Al_2O_3 and
850 TiO_2 contents of orthopyroxene in inclusion in chromite grains, in e) the XMg (100 ×

Mg/(Mg + Fe^{2+}) atomic ratio) and the TiO_2 content of amphibole in inclusion, and in f) the XNa (100 × Na/(Na + K) atomic ratio) of mica in inclusion. Coloured dots are averaged values per sample, depending on the chromite abundance in the sample, while small grey dots show the variability of un-averaged, analysed values. Blue lines are magmatic breccias.

Figure 8: Chemical profiles along the four samples 06OM04-3B2 (a), 06OM04-5D (b) and 06OM04-12E1 (d), all from the cross-section collected along the stratiform chromitite, and 04OM31E (c), collected near the base of the cross-section. For each profile along the thin section (about 3.5 cm in height) the variation of the chromite modal content is represented as well as of the XCr, Cr, Al and Fe^{3+} expressed in *apfu* (atom per formula unit, recalculated on the basis of O = 4), XMg and TiO_2 content of chromite, and of the Fo and NiO content of the surrounding matrix olivine.

Figure 9: Evolution of the Fo of olivine and XMg, XCr, YFe^{3+} and TiO_2 content of chromite in the samples 06OM04-3B2, 06OM04-5D, 06OM04-12E1 and 04OM31E depending on the modal content of chromite.

Figure 10: Comparison of the Fo and NiO content of olivine, between the matrix from chromitites from different areas in Oman, and in dunites from the Maqsad mantle-crust transition zone (Rospabé, 2018) and mantle harzburgites from the Sumail massif (Gerbert-Gaillard, 2002; Monnier et al., 2006; Quatrevaux, 1995). a) The Fo and NiO content are much higher in olivine matrix from the stratiform chromitite than in olivine from the surrounding DTZ or from mantle harzburgites. b) In the Sumail massif the high Fo and NiO values in matrix are shared both by DTZ chromitites (Rollinson, 2019; Zagrtdenov et al., 2018) and by mantle chromitites (Ceuleneer, unpublished data). In the northern massifs even more extreme

876 values were reported in the matrix from mantle chromitites (Miura et al., 2014; Rollinson,
877 2008, 2019, see also Augé, 1987) (no data about the olivine matrix composition in chromitites
878 outcropping within the mantle-crust transition zone in this area). Values were averaged for
879 each sample.
880
881 **Table 1.** Selected analyses of minerals from the matrix in chromitites and of silicate
882 inclusions in chromites (full dataset in Supplementary Material).
883
884 **References**

885 Abe, N., 2011. Petrology of podiform chromitite from the ocean floor at the 15° 20'N FZ in
886 the MAR, Site 1271, ODP Leg 209. J. Mineral. Petrol. Sci. 106, 97-102.
887 doi:10.2465/jmps.101022
888 Abily, B., Ceuleneer, G., 2013. The dunitic mantle-crust transition zone in the Oman
889 ophiolite: Residue of melt-rock interaction, cumulates from high-MgO melts, or both?
890 Geology 41, 67-70. doi:10.1130/G33351.1
891 Abily, B., Ceuleneer, G., Launeau, P., 2011. Synmagmatic normal faulting in the lower
892 oceanic crust: Evidence from the Oman ophiolite. Geology 39, 391-394.
893 doi:10.1130/G31652.1
894 Ahmed, A.H., Arai, S., 2002. Unexpectedly high-PGE chromitite from the deeper mantle
895 section of the northern Oman ophiolite and its tectonic implications. Contrib. to Mineral.
896 Petrol. 143, 263-278. doi:10.1007/s00410-002-0347-8
897 Amri, I., Benoit, M., Ceuleneer, G., 1996. Tectonic setting for the genesis of oceanic
898 plagiogranites: Evidence from a paleo-spreading structure in the Oman ophiolite. Earth
899 Planet. Sci. Lett. 139, 177-194. doi: 10.1016/0012-821X(95)00233-3
900 Arai, S., 1980. Dunite-harzburgite-chromitite complexes as refractory residue in the Sangun-

Yamaguchi zone, western Japan. J. Petrol. 21, 141-165. doi: 10.1093/petrology/21.1.141

Arai, S., Akizawa, N., 2014. Precipitation and dissolution of chromite by hydrothermal solutions in the Oman ophiolite: New behavior of Cr and chromite. Am. Mineral. 99, 28-34. doi:10.2138/am.2014.4473

Arai, S., Matsukage, K., 1998. Petrology of a chromitite micropod from Hess Deep, equatorial Pacific: a comparison between abyssal and alpine-type podiform chromitites. Lithos 43, 1-14. doi:10.1016/S0024-4937(98)00003-6

Arai, S., Yurimoto, H., 1994. Podiform chromitites of the Tari-Misaka ultramafic complex, southwestern Japan, as mantle-melt interaction products. Econ. Geol. 89, 1279-1288. doi: 10.2113/gsecongeo.89.6.1279

Benoit, M., Ceuleneer, G., Polvé, M., 1999. The remelting of hydrothermally altered peridotite at mid-ocean ridges by intruding mantle diapirs. Nature 402, 514-518. doi:10.1038/990073

Benoit, M., Polvé, M., Ceuleneer, G., 1996. Trace element and isotopic characterization of mafic cumulates in a fossil mantle diapir (Oman ophiolite). Chem. Geol. 134, 199-214. doi:10.1016/S0009-2541(96)00087-3

Borisova, A.Y., Ceuleneer, G., Kamenetsky, V.S., Arai, S., Béjina, F., Abily, B., Bindeman, I.N., Polvé, M., De Parseval, P., Aigouy, T., Pokrovski, G.S., 2012. A new view on the petrogenesis of the Oman ophiolite chromitites from microanalyses of chromite-hosted inclusions. J. Petrol. 53, 2411-2440. doi:10.1093/petrology/egs054

Boudier, F., Nicolas, A., 1995. Nature of the moho transition zone in the Oman ophiolite. J. Petrol. 36, 777-796. doi:10.1093/petrology/36.3.777

Bowen, N.L., 1928, The evolution of the igneous rocks. Princeton, N. J., Princeton Univ. Press, 332 p. (reprinted 1956 by Dover Pubs., Inc., N. Y.)

Bussolesi M., Grieco G., Tzamos E., 2019. Olivine-spinel diffusivity patterns in chromitites

926 and dunites from the Finero phlogopite-peridotite (Ivrea-Verbano Zone, Southern Alps):
927 implications for the thermal history of the massif. Minerals 9, 75.
928 doi:10.3390/min9020075
929 Cameron, E.N., 1975. Postcumulus and subsolidus equilibration of chromite and coexisting
930 silicates in the Eastern Bushveld Complex. Geochim. Cosmochim. Acta 39, 1021-1033.
931 doi:10.1016/0016-7037(75)90044-7
932 Cassard, D., Nicolas, A., Rabinovitch, M., Moutte, J., Leblanc, M., Prinzhofer, A., 1981.
933 Structural classification of chromite pods in southern New Caledonia. Econ. Geol. 76,
934 805-831. doi:10.2113/gsecongeo.76.4.805
935 Ceuleneer, G., 1991. Evidence for a Paleo-Spreading Center in the Oman Ophiolite: Mantle
936 Structures in the Maqsad Area. Springer Netherlands, pp. 147-173. doi:10.1007/978-94-
937 011-3358-6_9
938 Ceuleneer, G., Monnereau, M., Amri, I., 1996. Thermal structure of a fossil mantle diapir
939 inferred from the distribution of mafic cumulates. Nature 379, 149-153.
940 doi:10.1038/379149a0
941 Ceuleneer, G., Nicolas, A., 1985. Structures in podiform chromite from the Maqsad district
942 (Sumail ophiolite, Oman). Miner. Depos. 20, 177-184. doi:10.1007/BF00204562
943 Ceuleneer, G., Nicolas, A., Boudier, F., 1988. Mantle flow pattern at an oceanic spreading
944 centre: the Oman peridotite record. Tectonophysics 151, 1-26. doi:10.1016/0040-
945 1951(88)90238-7
946 Clénet H., Ceuleneer G., Pinet P., Abily B., Daydou Y., Harris E., Amri I. and Dantas C.,
947 2010. Thick sections of layered ultramafic cumulates in the Oman ophiolite revealed by
948 an airborne hyperspectral survey: petrogenesis and relationship to mantle diapirism.
949 Lithos, 114, 265-281. doi:10.1016/j.lithos.2009.09.002
950 Coleman, R.G., 1981. Tectonic setting for ophiolite obduction in Oman. J. Geophys. Res.

951 Solid Earth 86, 2497-2508. doi:10.1029/JB086iB04p02497
952 Evans, B.W., Frost, B.R., 1975. Chrome-spinel in progressive metamorphism - a preliminary
953 analysis. Geochim. Cosmochim. Acta 39, 959-972. doi: 10.1016/B978-0-08-019954-
954 2.50020-2
955 Fabriès, J., 1979. Spinel-olivine geothermometry in peridotites from ultramafic complexes.
956 Contrib. to Mineral. Petrol. 69, 329-336. doi:10.1007/BF00372258
957 Gauthier, M., Corrivaux, L., Trottier, L.J., Cabri, J., Laflamme, J.G., Bergeron, M., 1990.
958 Chromitites platinifères des complexes ophiolitiques de l'Estrie-Beauce, Appalaches du
959 Sud du Québec. Miner. Depos. 25, 169-178. doi:10.1007/BF00190378
960 Gerbert-Gaillard, L., 2002. Caractérisation géochimique des péridotites de l'ophiolite
961 d'Oman: processus magmatiques aux limites lithosphère/asthénosphère. PhD thesis,
962 Université Montpellier II - Sciences et Techniques du Languedoc.
963 Glennie, K.W., Boeuf, M.G.A., Clarke, M.H., Moody-Stuart, M., Pilaar, W.F.H., Reinhardt,
964 B.M., 1973. Late Cretaceous nappes in Oman Mountains and their geologic evolution.
965 Am. Assoc. Pet. Geol. Bull. 57, 5-27.
966 González-Jiménez, J.M., Griffin, W.L., Proenza, J.A., Gervilla, F., O'Reilly, S.Y., Akbulut,
967 M., Pearson, N.J., Arai, S., 2014. Chromitites in ophiolites: how, where, when, why?
968 Part II. The crystallization of chromitites. Lithos, 189, 140-158.
969 Grieco, G., Bussolesi, M., Tzamos, E., Rassios, A.E., Kapsiotis, A., 2018. Processes of
970 primary and re-equilibration mineralization affecting chromitite ore geochemistry within
971 the Vourinos ultramafic sequence, Vourinos ophiolite (West Macedonia, Greece). Ore
972 Geol. Rev. 95, 537-551. doi:10.1016/j.oregeorev.2018.03.009
973 Irvine, T.N., 1977a. Origin of chromitite layers in the Muskox intrusion and other stratiform
974 intrusions: A new interpretation. Geology 5, 273-277. doi:10.1130/0091-
975 7613(1977)5<273:OOCLIT>2.0.CO;2

976 Irvine, T.N., 1977b. Chromite crystallization in the join Mg_2SiO_4-$CaMgSi_2O_6$-$CaAl_2Si_2O_8$-
977 $MgCr_2O_4$-SiO_2. Carnegie Instite. Washington Yearbook 76, 465-472.
978 Irvine, T.N., 1975. Crystallization sequences in the Muskox intrusion and other layered
979 intrusions-II. Origin of chromitite layers and similar deposits of other magmatic ores.
980 Geochim. Cosmochim. Acta 39, 991-1020. doi:10.1016/0016-7037(75)90043-5
981 Jackson E.D., 1961. Primary textures and mineral associations in the ultramafic zone of the
982 Stillwater complex, Montana. U.S. Geol. Surv. Prof. Paper 358, 106 pp.
983 Johan, Z., Dunlop, H., Le Bel, L., Robert, J.L., Volfinger, M., 1983. Origin of chromite
984 deposits in ophiolitic complexes: evidence for a volatile- and sodium-rich reducing fluid
985 phase. Fortschr. Mineral. 61, 105-107.
986 Johan, Z., Martin, R.F., Ettler, V., 2017. Fluids are bound to be involved in the formation of
987 ophiolitic chromite deposits. Eur. J. Mineral. 29, 543-555. doi:10.1127/ejm/2017/0029-
988 2648
989 Koepke, J., Berndt, J., Horn, I., Fahle, J., Wolff, P.E., 2014. Partial melting of oceanic gabbro
990 triggered by migrating water-rich fluids: A prime example from the Oman Ophiolite.
991 Geol. Soc. Lond. 392, 195-212 (Spec. Publ.). doi:10.1144/SP392.10
992 Koepke, J., Feig, S.T., Snow, J., 2005. Hydrous partial melting within the lower oceanic crust.
993 Terra Nova 17, 286-291. doi:10.1111/j.1365-3121.2005. 00613.x
994 Koga, K.T., Kelemen, P.B., Shimizu, N., 2001. Petrogenesis of the crust-mantle transition
995 zone and the origin of lower crustal wehrlite in the Oman ophiolite. Geochemistry,
996 Geophys. Geosystems 2. doi:10.1029/2000GC000132
997 Lago B., Rabinowicz M., Nicolas A., 1982. Podiform chromite ore bodies - a genetic model.
998 J. Petrol. 23, 103-125. doi:10.1093/petrology/23.1.103
999 Latypov, R., Costin, G., Chistyakova, S., Hunt, E. J., Mukherjee, R., Naldrett, T., 2018.
1000 Platinum-bearing chromite layers are caused by pressure reduction during magma ascent.

1001 Nat. com. 9, 462. doi:10.1038/s41467-017-02773-w
1002 Leblanc, M., Ceuleneer, G., 1991. Chromite crystallization in a multicellular magma flow:
1003 Evidence from a chromitite dike in the Oman ophiolite. Lithos 27, 231-257.
1004 doi:10.1016/0024-4937(91)90002-3
1005 Lehmann, J., 1983. Diffusion between olivine and spinel: application to geothermometry.
1006 Earth Planet. Sci. Lett. 64, 123-138. doi:10.1016/0012-821X(83)90057-2
1007 Lipin, B. R., 1993. Pressure increases, the formation of chromite seams, and the development
1008 of the ultramafic series in the Stillwater Complex, Montana. J. Petrol. 34, 955-976.
1009 doi:10.1093/petrology/34.5.955.
1010 Lombaard, B.V., 1956. Chromite and dunite of the Bushveld Complex. South Afr. J. Geol.
1011 59, 59-74.
1012 Lorand J.-P. and Ceuleneer G., 1989. Silicate and base-metal sulfide inclusions in chromites
1013 from the Maqsad area (Oman ophiolite, Gulf of Oman): a model for entrapment. Lithos,
1014 22, 173-190.
1015 Matsukage, K., Arai, S., 1998. Jadeite, albite and nepheline as inclusions in spinel of
1016 chromitite from Hess Deep, equatorial Pacific: their genesis and implications for
1017 serpentinite diapir formation. Contrib. to Mineral. Petrol. 131, 111-122.
1018 doi:10.1007/s004100050382
1019 Mathez, E.A., Kinzler, R.J., 2017. Metasomatic chromitite seams in the Bushveld and Rum
1020 Layered intrusions. Elements, 13, 397-402.
1021 Matveev, S., Ballhaus, C., 2002. Role of water in the origin of podiform chromitite deposits.
1022 Earth Planet. Sci. Lett. 203, 235-243. doi:10.1016/S0012-821X(02)00860-9
1023 McElduff, B., Stumpfl, E.F., 1991. The chromite deposits of the Troodos complex, Cyprus-
1024 evidence for the role of a fluid phase accompanying chromite formation. Miner. Depos.
1025 26, 307-318. doi:10.1007/BF00191079

1026 Miura, M., Arai, S., Tamura, A., 2014. Formation of discordant chromitite at the initiation of
1027 sub-arc mantle processes: Observations from the northern Oman ophiolite. J. Mineral.
1028 Petrol. Sci. 109, 38-43. doi:10.2465/jmps.131006
1029 Mondal, S. K., Mathez, E. A., 2006. Origin of the UG2 chromitite layer, Bushveld Complex.
1030 J. Petrol. 48, 495-510. doi:10.1093/petrology/egl069
1031 Monnier, C., Girardeau, J., Le Mée, L., Polvé, M., 2006. Along-ridge petrological
1032 segmentation of the mantle in the Oman ophiolite. Geochemistry, Geophys. Geosystems.
1033 doi:10.1029/2006GC001320
1034 Montigny, R., Le Mer, O., Thuizat, R., Whitechurch, H., 1988. K-Ar and 40Ar39Ar study of
1035 metamorphic rocks associated with the Oman ophiolite: Tectonic implications.
1036 Tectonophysics 151, 345-362. doi:10.1016/0040-1951(88)90252-1
1037 Naldrett, A. J., Wilson, A., Kinnaird, J., Yudovskaya, M., Chunnett, G., 2012. The origin of
1038 chromitites and related PGE mineralization in the Bushveld Complex: new mineralogical
1039 and petrological constraints. Mineralium Deposita 47, 209-232. doi:10.1007/s00126-
1040 011-0366-3
1041 Nonnotte, P., Ceuleneer, G., Benoit, M., 2005. Genesis of andesitic-boninitic magmas at mid-
1042 ocean ridges by melting of hydrated peridotites: Geochemical evidence from DSDP Site
1043 334 gabbronorites. Earth Planet. Sci. Lett. 236, 632-653. doi:10.1016/j.epsl.2005.05.026
1044 O'Neill, H.S.C., Wall, V.J., 1987. The olivine - orthopyroxene - spinel oxygen geobarometer,
1045 the nickel precipitation curve, and the oxygen fugacity of the earth's upper mantle. J.
1046 Petrol. 28, 1169-1191. doi:10.1093/petrology/28.6.1169
1047 Payot, B.D., Arai, S., Dick, H.J., Abe, N., Ichiyama, Y., 2014. Podiform chromitite formation
1048 in a low-Cr/high-Al system: An example from the Southwest Indian Ridge (SWIR).
1049 Mineral. Petrol. 108, 533-549. doi:10.1007/s00710-0134-0317-z
1050 Pearce, J.A., Alabaster, T., Shelton, A.W., Searle, M.P., 1981. The Oman ophiolite as a

1051 Cretaceous arc-basin complex: evidence and implications. Philos. Trans. R. Soc. London
1052 300, 299-317. doi:10.1098/rsta.1892.0001
1053 Pouchou, J.-L., Pichoir, F., 1985. “PAP” phi-rho-Z procedure for improved quantitative
1054 microanalysis., in: Armstrong, J. (Ed.), Microbeam Analysis. San Francisco, CA, pp.
1055 104-106.
1056 Python, M., Ceuleneer, G., 2003. Nature and distribution of dykes and related melt migration
1057 structures in the mantle section of the Oman ophiolite. Geochemistry, Geophys.
1058 Geosystems 4. doi:10.1029/2003GC000354
1059 Python, M., Ceuleneer, G., Arai, S., 2008. Chromian spinels in mafic-ultramafic mantle
1060 dykes: Evidence for a two-stage melt production during the evolution of the Oman
1061 ophiolite. Lithos 106, 137-154. doi:10.1016/j.lithos.2008.07.001
1062 Python, M., Ceuleneer, G., Ishida, Y., Barrat, J.-A., Arai, S., 2007. Oman diopsidites: a new
1063 lithology diagnostic of very high temperature hydrothermal circulation in mantle
1064 peridotite below oceanic spreading centres. Earth Planet. Sci. Lett. 255, 289-305.
1065 doi:10.1016/j.epsl.2006.12.030
1066 Quatrevaux, F., 1995. Etude pétrologique des péridotites des massifs de Maqsad et Wuqbah,
1067 ophiolite d’Oman. PhD thesis, Université Paris 7.
1068 Rabinowicz, M., Ceuleneer, G., Nicolas, A., 1987. Melt segregation and flow in mantle
1069 diapirs below spreading centres: evidence from the Oman ophiolite. J. Geophys. Res.
1070 Solid Earth 92, 3475-3486. doi:10.1029/JB092iB05p03475
1071 Rahgoshay, M., Juteau, T., Whitechurch, H., 1981. Kizilyuksek Tepe: un gisement
1072 exceptionnel de chromite stratiforme dans un complexe ophiolitique (massif de Pozanti-
1073 Karsanti, Taurus, Turquie). C.R. Acad. Sc. Paris 293, 765-770
1074 Rioux, M., Bowring, S., Kelemen, P., Gordon, S., Miller, R., Dudás, F., 2013. Tectonic
1075 development of the Samail ophiolite: High-precision U-Pb zircon geochronology and

1076 Sm-Nd isotopic constraints on crustal growth and emplacement. J. Geophys. Res. Solid
1077 Earth 118, 2085-2101. doi:10.1002/jgrb.50139
1078 Rioux, M., Garber, J., Bauer, A., Bowring, S., Searle, M., Kelemen, P., Hacker, B., 2016.
1079 Synchronous formation of the metamorphic sole and igneous crust of the Semail
1080 ophiolite: New constraints on the tectonic evolution during ophiolite formation from
1081 high-precision U-Pb zircon geochronology. Earth Planet. Sci. Lett. 451, 185-195.
1082 doi:10.1016/j.epsl.2016.06.051
1083 Rollinson, H., 2019. Dunites in the mantle section of the Oman ophiolite-the boninite
1084 connection. Lithos. doi:10.1016/j.lithos.2019.03.008
1085 Rollinson, H., 2008. The geochemistry of mantle chromitites from the northern part of the
1086 Oman ophiolite: Inferred parental melt compositions. Contrib. to Mineral. Petrol. 156,
1087 273-288. doi:10.1007/s00410-008-0284-2
1088 Rollinson, H., Adetunji, J., 2015. Chromite in the Mantle Section of the Oman Ophiolite:
1089 Implications for the Tectonic Evolution of the Oman Ophiolite. Acta Geol. Sin.
1090 doi:10.1111/1755-6724.12308_44
1091 Rollinson, H., Adetunji, J., 2013. Mantle podiform chromitites do not form beneath mid-
1092 ocean ridges: A case study from the Moho transition zone of the Oman ophiolite. Lithos
1093 177, 314-327. doi:10.1016/j.lithos.2013.07.004
1094 Rollinson, H., Mameri, L., Barry, T., 2018. Polymineralic inclusions in mantle chromitites
1095 from the Oman ophiolite indicate a highly magnesian parental melt. Lithos 310, 381-391.
1096 doi:10.1016/j.lithos.2018.04.024
1097 Rospabé, M., 2018. Etude pétrologique, géochimique et structurale de la zone de transition
1098 dunitique dans l'ophiolite d'Oman : Identification des processus pétrogénétiques à
1099 l'interface manteau/croûte. PhD thesis, Université Paul Sabatier, Toulouse III.
1100 Rospabé, M., Benoit, M., Ceuleneer, G., Hodel, F., Kaczmarek, M.-A., 2018. Extreme

1101 geochemical variability through the dunitic transition zone of the Oman ophiolite:
1102 Implications for melt/fluid-rock reactions at Moho level beneath oceanic spreading
1103 centers. Geochim. Cosmochim. Acta 234, 1-23. doi:10.1016/j.gca.2018.05.012
1104 Rospabé, M., Benoit, M., Ceuleneer, G., Kaczmarek, M.-A., Hodel, F., 2019. Melt
1105 hybridization and metasomatism triggered by syn-magmatic faults within the Oman
1106 ophiolite: A clue to understand the genesis of the dunitic mantle-crust transition zone.
1107 Earth Planet. Sci. Lett. 516, 108-121. doi:10.1016/j.epsl.2019.04.004
1108 Rospabé, M., Ceuleneer, G., Benoit, M., Abily, B., Pinet, P., 2017. Origin of the dunitic
1109 mantle-crust transition zone in the Oman ophiolite: The interplay between percolating
1110 magmas and hightemperature hydrous fluids. Geology 45, 471-474.
1111 doi:10.1130/G38778.1
1112 Schiano, P., Clocchiatti, R., Lorand, J. P., Massare, D., Deloule, E., Chaussidon, M., 1997.
1113 Primitive basaltic melts included in podiform chromites from the Oman Ophiolite. Earth
1114 Planet. Sci. Lett. 146, 489-497. doi:10.1016/S0012-821X(96)00254-3
1115 Spandler, C., Mavrogenes, J., Arculus, R., 2005. Origin of chromitites in layered intrusions:
1116 Evidence from chromite-hosted melt inclusions from the Stillwater Complex. Geology
1117 33, 893-896. doi:10.1130/G21912.1
1118 Stoll, W.C., 1958. Geology and Petrology of the Masinloc chromite deposit Zambales, Luzon,
1119 Philippine Islands. Geol. Soc. Am. Bull. 69, 419-448. doi:10.1130/0016-
1120 7606(1958)69[419:GAPOTM]2.0.CO;2
1121 Talkington, R.W., Watkinson, D.H., Whittaker, P.J., Jones, P.C., 1984. Platinum-group
1122 minerals and other solid inclusions in chromite of ophiolitic complexes: occurrence and
1123 petrological significance. Tschermaks Mineral. Petr. Mitt. 32, 285-301.
1124 doi:10.1007/BF01081619
1125 Tamura, A., Morishita, T., Ishimaru, S., Arai, S., 2014. Geochemistry of spinel-hosted

amphibole inclusions in abyssal peridotite: insight into secondary melt formation in melt–peridotite reaction. Contrib. to Mineral. Petrol. 167, 974. doi:10.1007/s00410-014-0974-x

Thayer, T.P., 1960. Some critical differences between alpine type and stratiform peridotite-gabbro complexes. Int. Geol. Congr. 21th 13, 247-259.

Tippit, P.R., Pessagno, E.A., Smewing, J.D., 1981. The Biostratigraphy of Sediments in the Volcanic Unit of the Samail Ophiolite. J. Geophys. Res. Solid Earth 86, 2756-2762. doi:10.1029/JB086iB04p02756

Warren, C.J., Parrish, R.R., Waters, D.J., Searle, M.P., 2005. Dating the geologic history of Oman's Semail ophiolite: Insights from U-Pb geochronology. Contrib. to Mineral. Petrol. 150, 403-422. doi:10.1007/s00410-005-0028-5

Zagrtdenov, N.R., Ceuleneer, G., Rospabé, M., Borisova, A.Y., Toplis, M.J., Benoit, M., Abily, B., 2018. Anatomy of a chromitite dyke in the mantle/crust transition zone of the Oman ophiolite. Lithos 312-313. doi:10.1016/j.lithos.2018.05.012

Zhou, M.F., Robinson, P.T., Bai, W.J., 1994. Formation of podiform chromitites by melt/rock interaction in the upper mantle. Miner. Depos. 29, 98-101. doi:10.1007/BF03326400

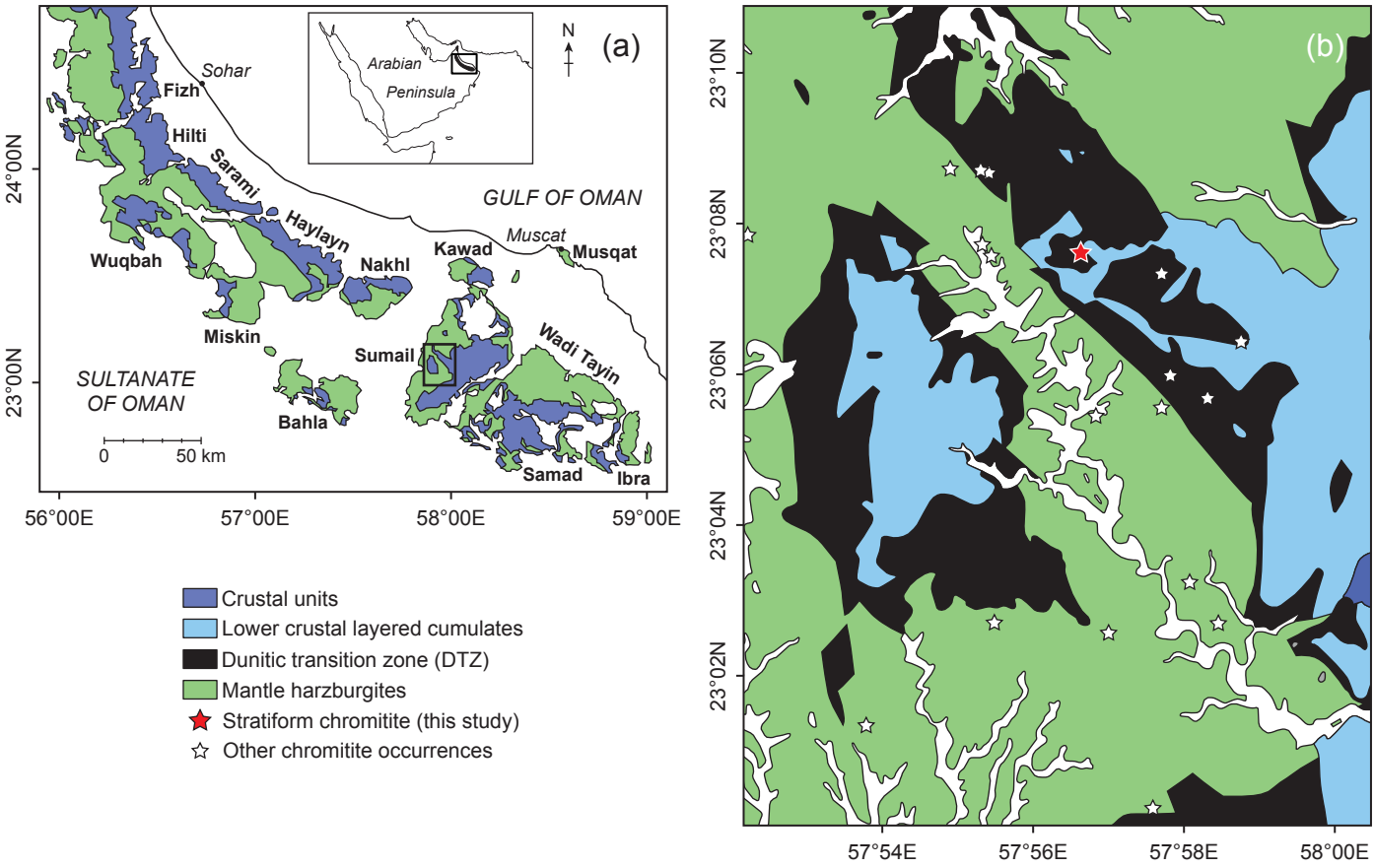
(a)
N
Arabian
Peninsula
Sohar
Fizh
Hilti
Sarami
Haylayn
Wuqbah
Nakhl
Kawad
Muscat
Musqat
GULF OF OMAN
Miskin
Sumail
Wadi Tayin
SULTANATE
OF OMAN
Bahla
Samad
Ibra
0
50 km
24°00N
23°00N
56°00E
57°00E
58°00E
59°00E
(b)
23°10N
23°08N
23°06N
23°04N
23°02N
57°54E
57°56E
57°58E
58°00E
Crustal units
Lower crustal layered cumulates
Dunitic transition zone (DTZ)
Mantle harzburgites
Stratiform chromitite (this study)
Other chromitite occurrences

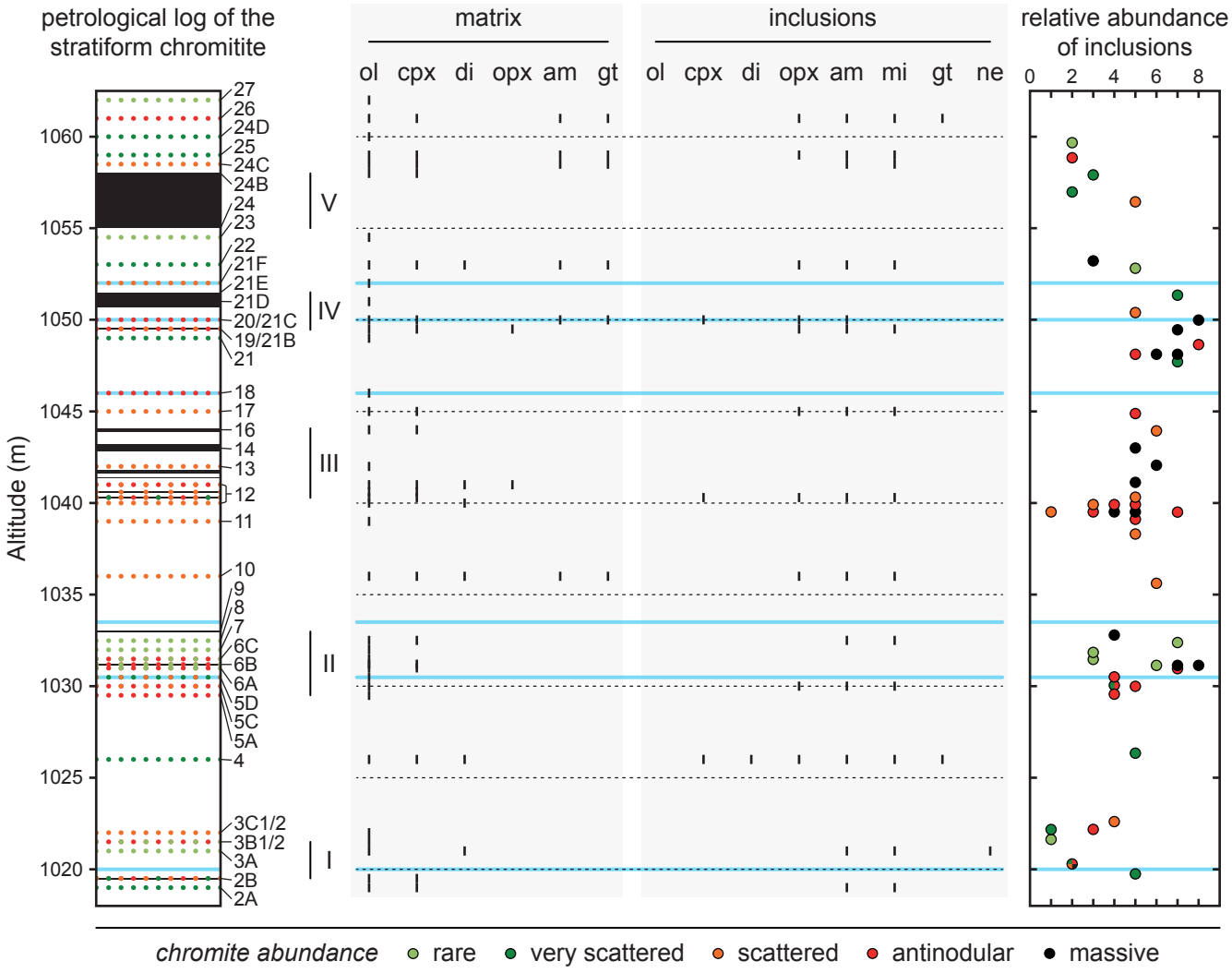
petrological log of the stratiform chromitite
matrix
inclusions
relative abundance of inclusions
ol cpx di opx am gt
ol cpx di opx am mi gt ne
0 2 4 6 8
Altitude (m)
1060
1055
1050
1045
1040
1035
1030
1025
1020
27
26
24D
25
24C
24B
24
23
22
21F
21E
21D
20/21C
19/21B
21
18
17
16
14
13
12
11
10
9
8
7
6C
6B
6A
5D
5C
5A
4
3C1/2
3B1/2
3A
2B
2A
V
IV
III
II
I
chromite abundance
rare
very scattered
scattered
antinodular
massive

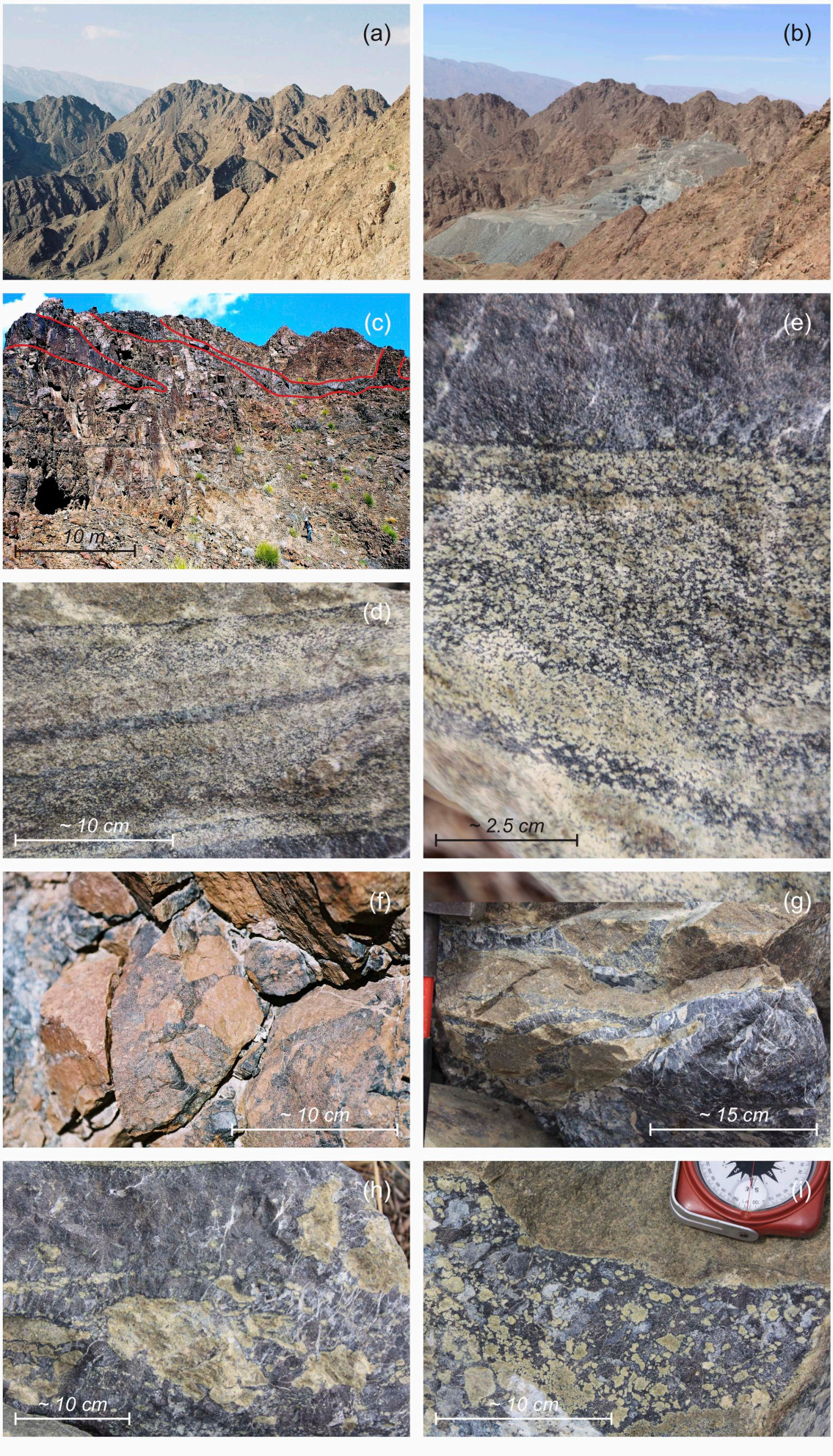
(a)
(b)
(c)
~ 10 m
(e)
~ 2.5 cm
(d)
~ 10 cm
(f)
~ 10 cm
(g)
~ 15 cm
(h)
~ 10 cm
(i)
~ 10 cm

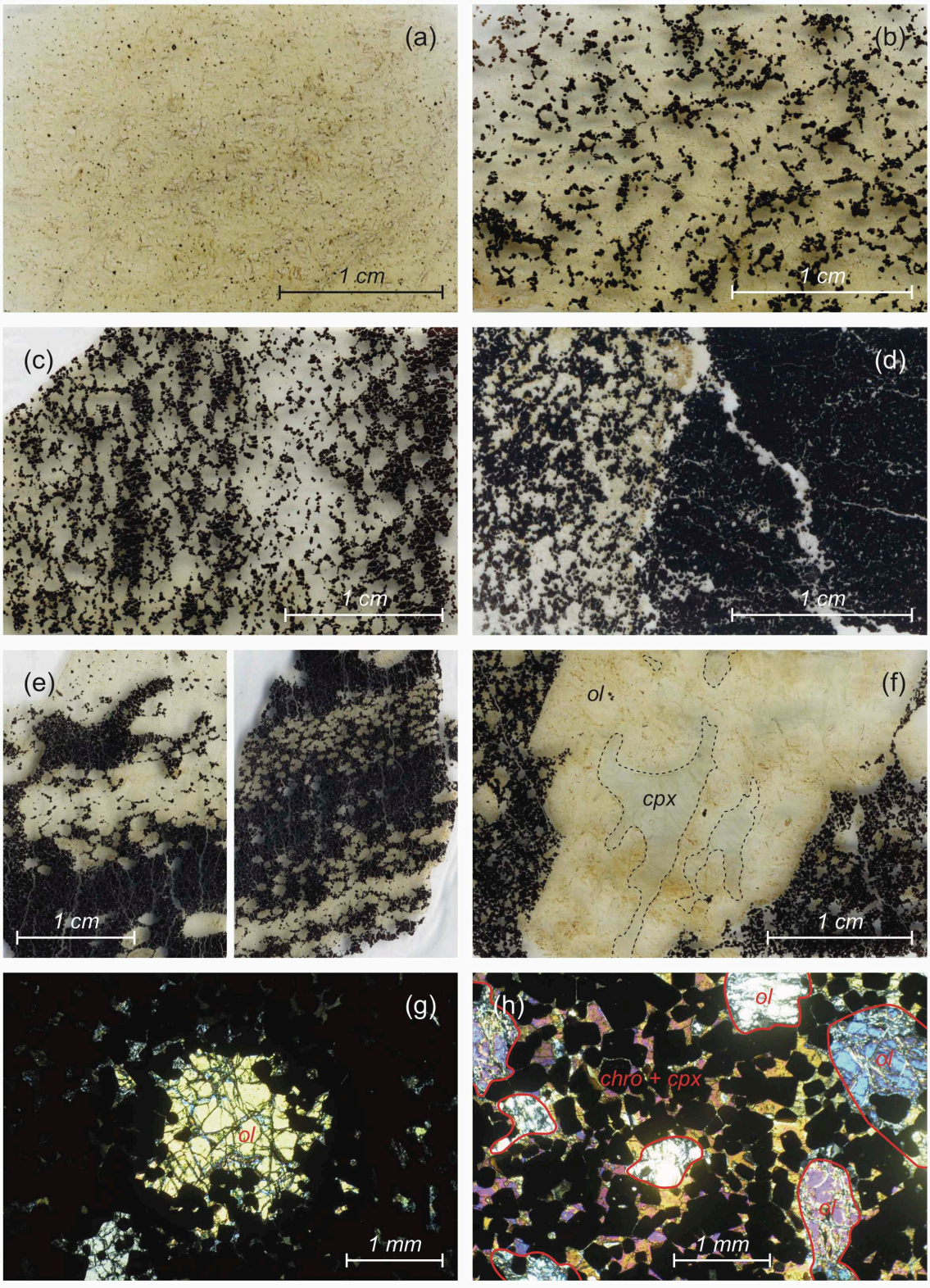
(a)
1 cm
(b)
1 cm
(c)
1 cm
(d)
1 cm
(e)
1 cm
(f)
ol
cpx
1 cm
(g)
ol
1 mm
(h)
ol
chro + cpx
ol
ol
1 mm

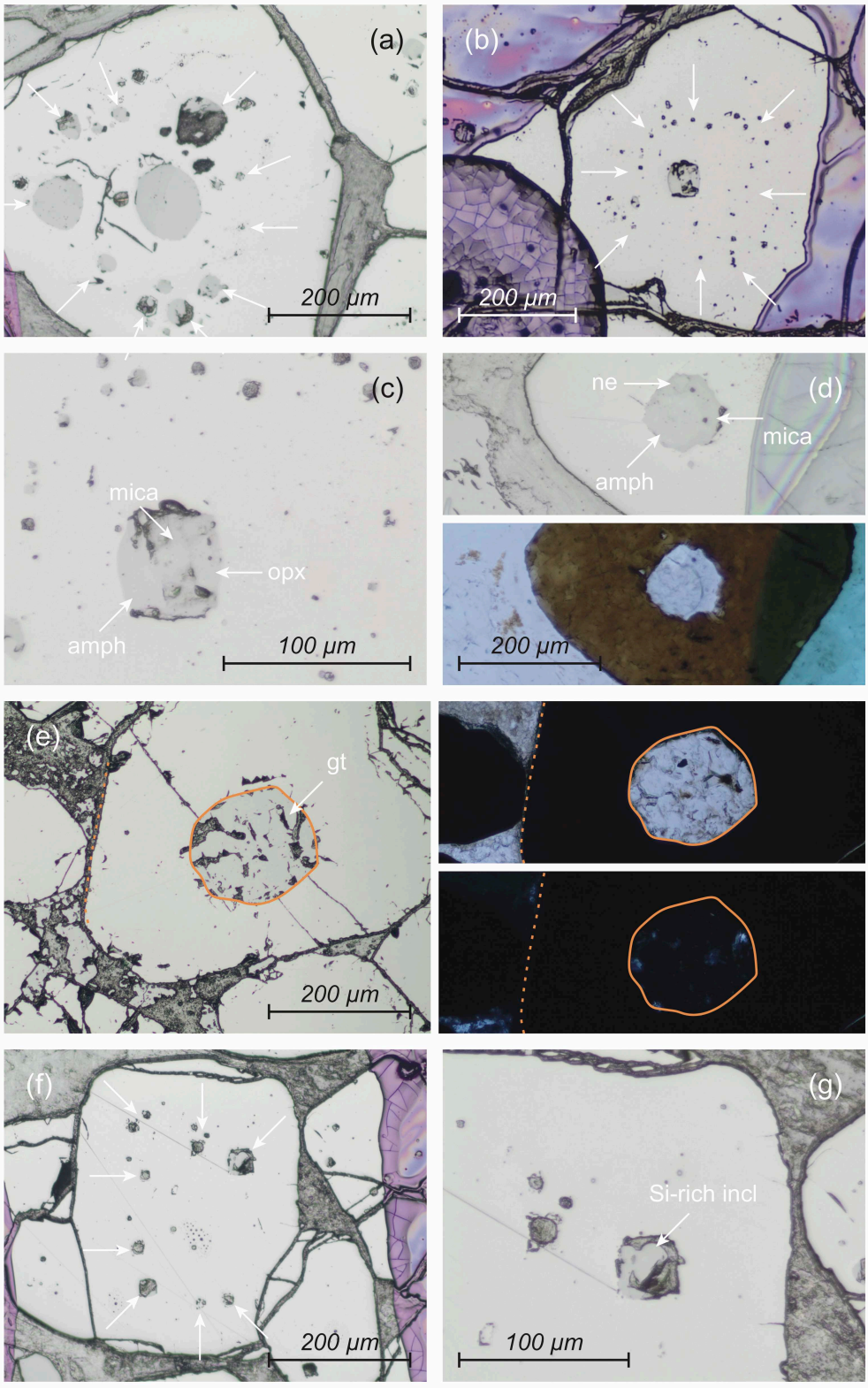
(a)
200 µm
(b)
200 µm
(c)
mica
opx
amph
100 µm
ne
(d)
mica
amph
200 µm
(e)
gt
200 µm
(f)
200 µm
(g)
Si-rich incl
100 µm

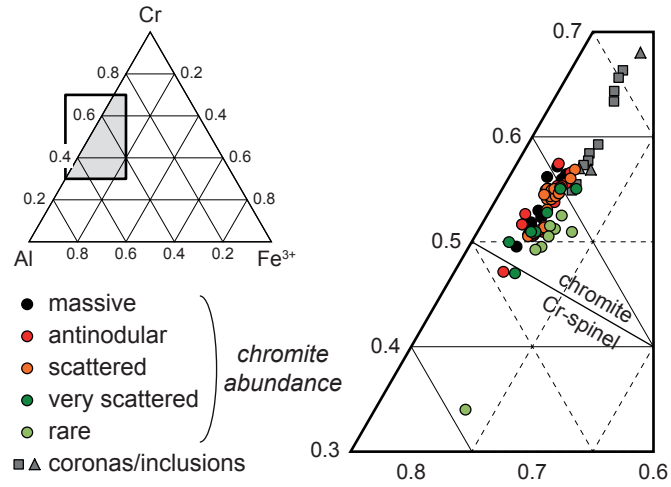
Cr
Al
Fe3+
0.8
0.6
0.4
0.2
massive
antinodular
scattered
very scattered
rare
coronas/inclusions
chromite abundance
chromite
Cr-spinel
0.7
0.6
0.5
0.4
0.3

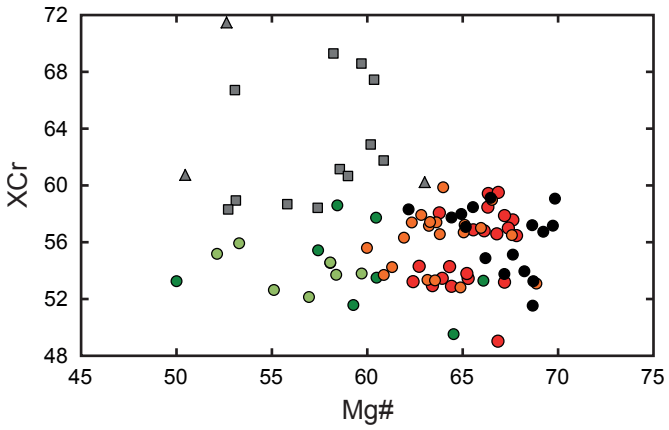
XCr
Mg#
72
68
64
60
56
52
48
45
50
55
60
65
70
75

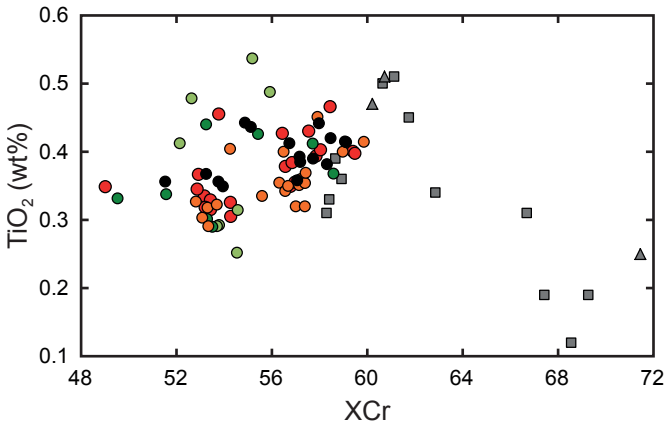
TiO2 (wt%)
XCr
0.6
0.5
0.4
0.3
0.2
0.1
48
52
56
60
64
68
72

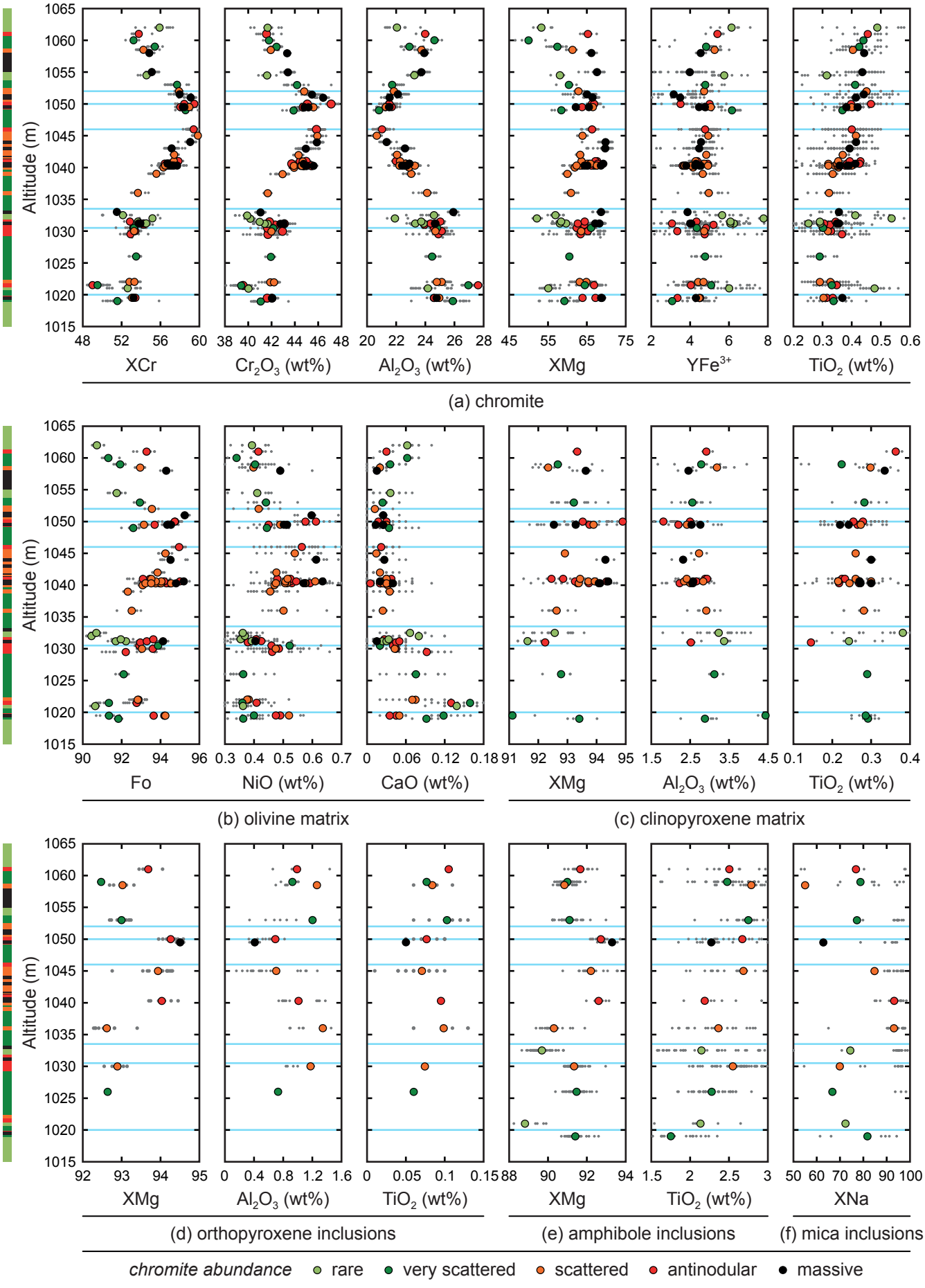
Altitude (m)
1065
1060
1055
1050
1045
1040
1035
1030
1025
1020
1015
XCr
48 52 56 60
Cr2O3 (wt%)
38 40 42 44 46 48
Al2O3 (wt%)
20 22 24 26 28
XMg
45 55 65 75
YFe3+
2 4 6 8
TiO2 (wt%)
0.2 0.3 0.4 0.5 0.6
(a) chromite
Fo
90 92 94 96
NiO (wt%)
0.3 0.4 0.5 0.6 0.7
CaO (wt%)
0 0.06 0.12 0.18
(b) olivine matrix
XMg
91 92 93 94 95
Al2O3 (wt%)
1.5 2.5 3.5 4.5
TiO2 (wt%)
0.1 0.2 0.3 0.4
(c) clinopyroxene matrix
XMg
92 93 94 95
Al2O3 (wt%)
0 0.4 0.8 1.2 1.6
TiO2 (wt%)
0 0.05 0.1 0.15
(d) orthopyroxene inclusions
XMg
88 90 92 94
TiO2 (wt%)
1.5 2 2.5 3
(e) amphibole inclusions
XNa
50 60 70 80 90 100
(f) mica inclusions
chromite abundance
rare
very scattered
scattered
antinodular
massive

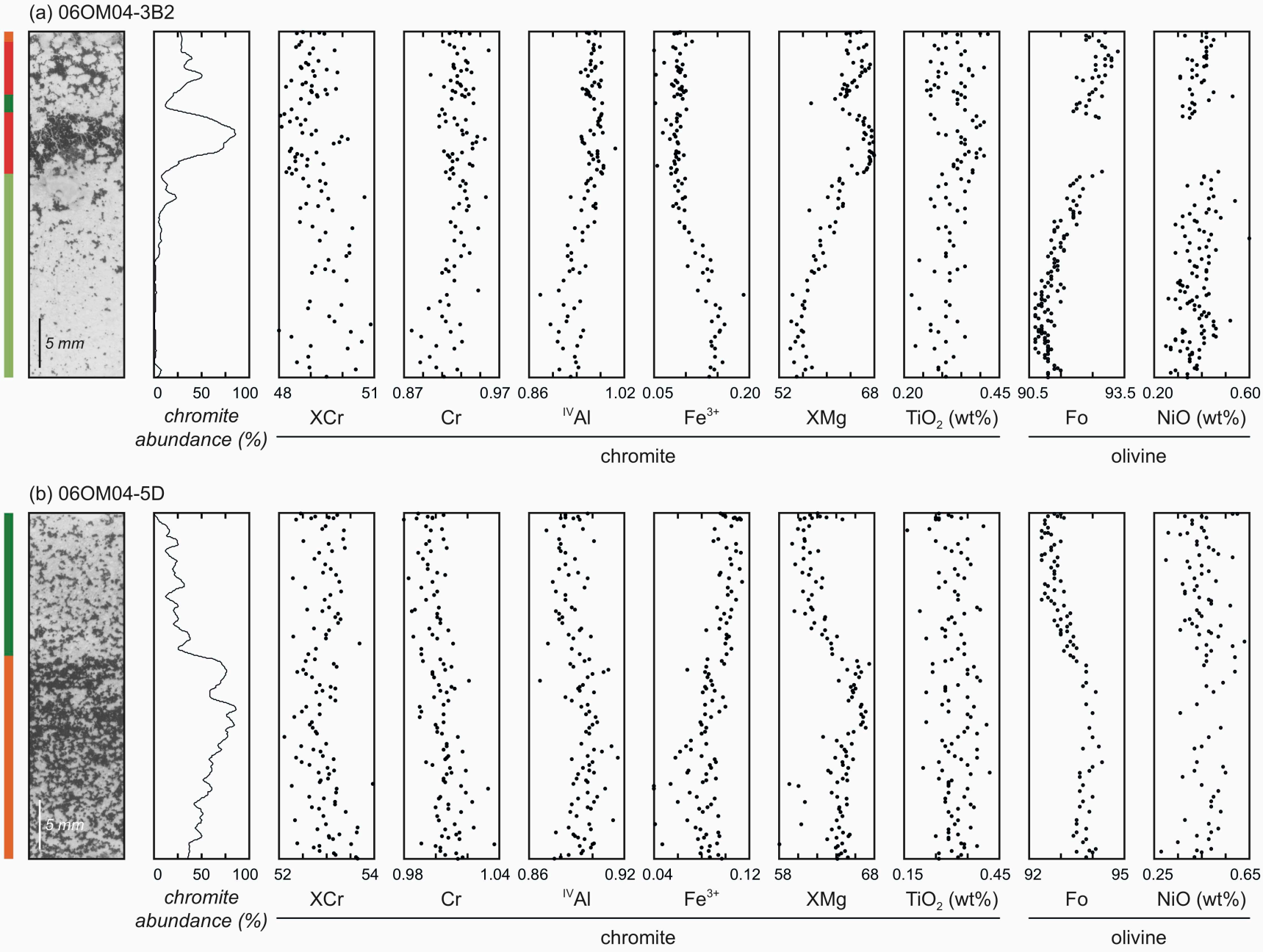
(a) 06OM04-3B2
5 mm
0 50 100
chromite abundance (%)
48 51
XCr
0.87 0.97
Cr
0.86 1.02
IVAl
0.05 0.20
Fe3+
52 68
XMg
0.20 0.45
TiO2 (wt%)
90.5 93.5
Fo
0.20 0.60
NiO (wt%)
chromite
olivine
(b) 06OM04-5D
5 mm
0 50 100
chromite abundance (%)
52 54
XCr
0.98 1.04
Cr
0.86 0.92
IVAl
0.04 0.12
Fe3+
58 68
XMg
0.15 0.45
TiO2 (wt%)
92 95
Fo
0.25 0.65
NiO (wt%)
chromite
olivine

(c) 04OM31E

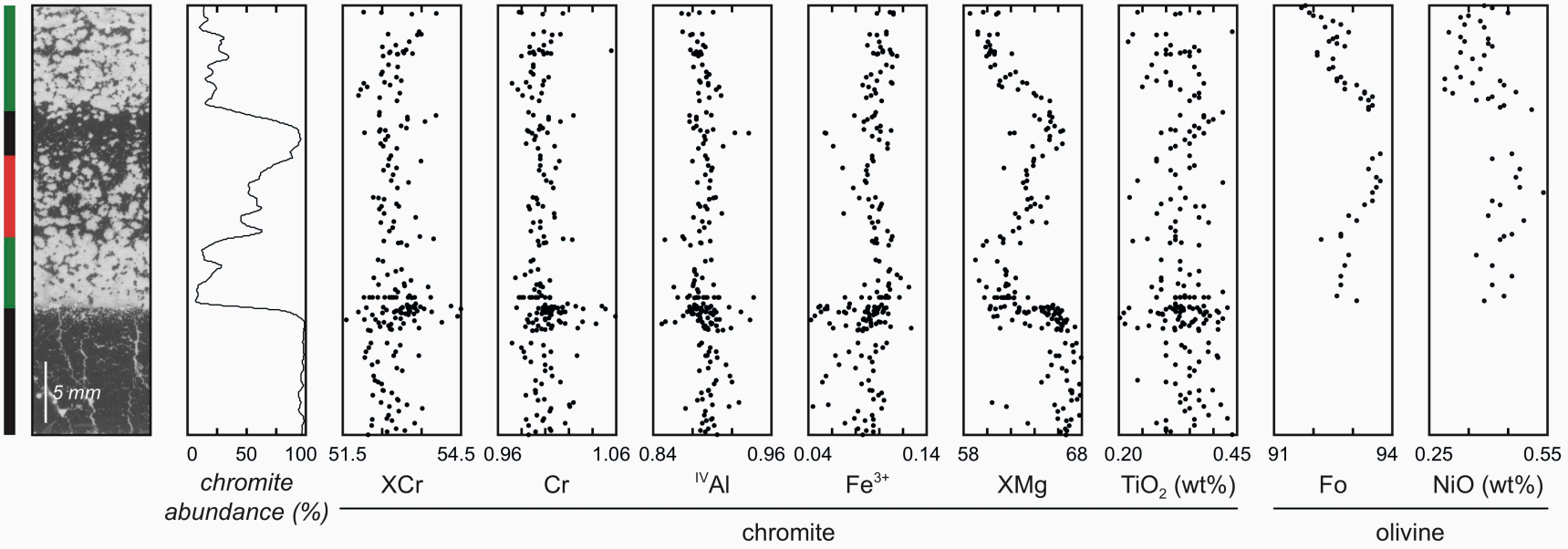

(d) 06OM04-12E1

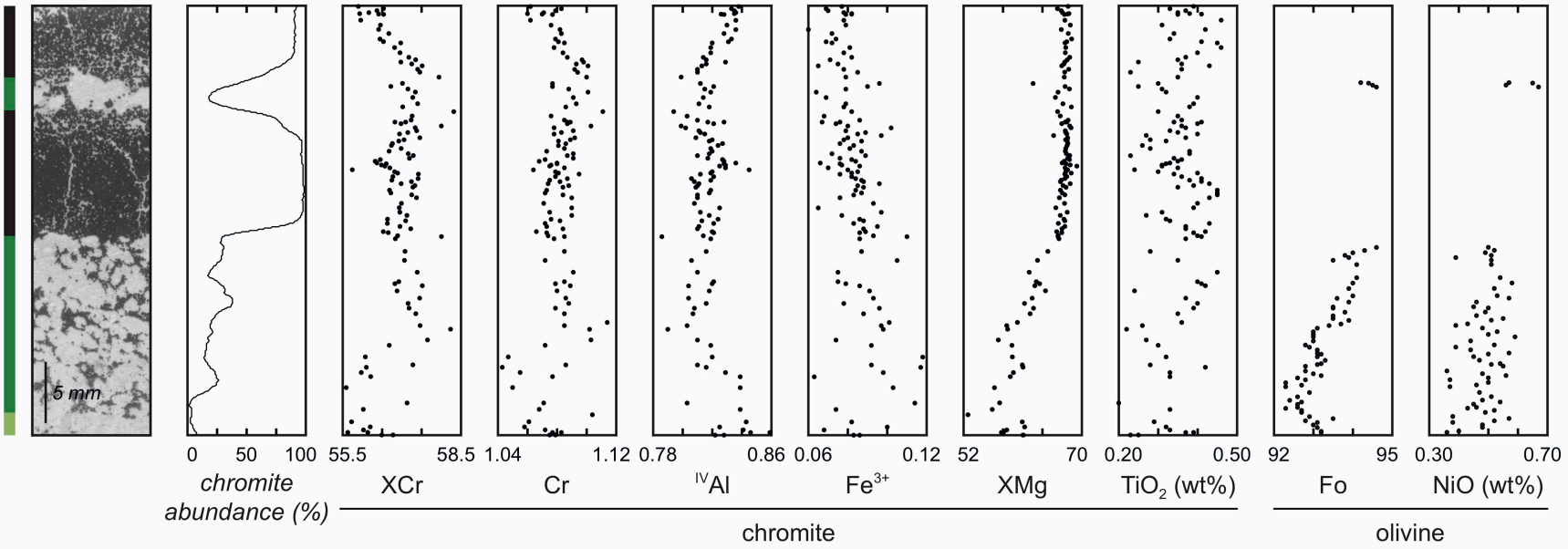

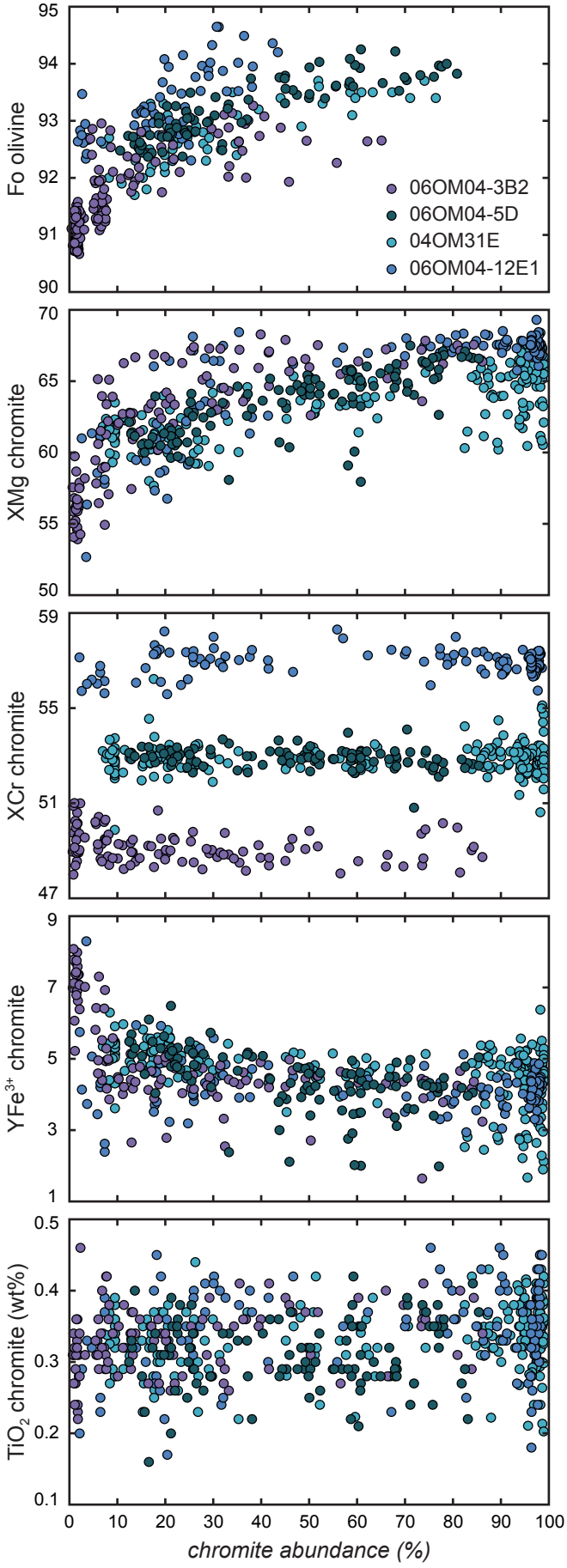
Fo olivine
XMg chromite
XCr chromite
YFe3+ chromite
TiO2 chromite (wt%)
chromite abundance (%)
06OM04-3B2
06OM04-5D
04OM31E
06OM04-12E1

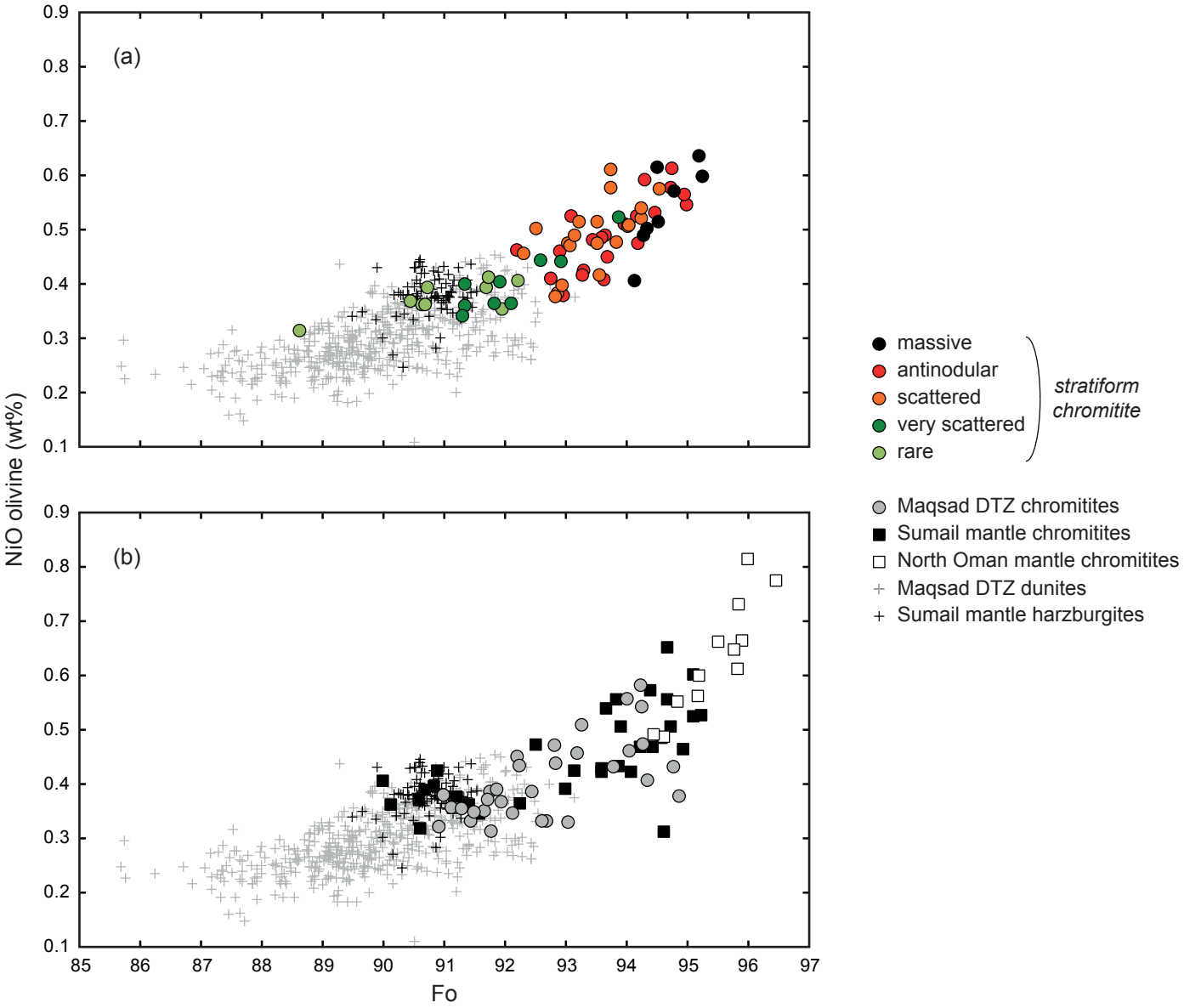
(a)
(b)
NiO olivine (wt%)
Fo
0.9
0.8
0.7
0.6
0.5
0.4
0.3
0.2
0.1
85
86
87
88
89
90
91
92
93
94
95
96
97
massive
antinodular
scattered
very scattered
rare
stratiform chromitite
Maqsad DTZ chromitites
Sumail mantle chromitites
North Oman mantle chromitites
Maqsad DTZ dunites
Sumail mantle harzburgites

Table 1. Selected analyses of minerals from the matrix in chromitites and of silicate inclusions in chromites (full dataset in Supplementary Material).

Sample	06OM04-2A	06OM04-1	06OM04-4	06OM04-12B2C		06OM04-12E1	06OM04-20		06OM04-5C2	06OM04-10	06OM04-3A
Chromite abundance	very scattered	rare	very scattered	antinodular		massive / antinodular	antinodular		scattered	scattered	rare
Mineral	Chro	Ol	Opx	Cpx		Diop	Amph		Mica (asp.)	Garnet (gr.)	Neph
Mode of occurrence	matrix	matrix	inclusion	matrix	inclusion	matrix	matrix	inclusion	inclusion	matrix	inclusion
SiO_2	0.05	40.90	57.42	52.35	52.69	54.89	45.86	44.81	40.97	39.41	46.51
TiO_2	0.34		0.06	0.27	0.28	0.16	1.47	3.42	4.37	0.04	0.04
Al_2O_3	25.89		0.73	2.53	2.38	0.79	11.37	10.78	16.45	21.14	32.63
Cr_2O_3	41.09	0.02	0.97	1.34	1.46	0.37	1.68	2.69	2.29	1.36	0.62
FeO_{total}	18.34	11.02	5.01	2.13	2.01	0.84	2.73	2.53	2.19	0.78	0.39
MnO	0.25	0.20	0.17	0.08	0.03	0.15	0.06		0.01	0.10	
MgO	12.99	48.23	35.37	17.74	16.94	18.05	18.57	18.08	23.34	0.52	0.77
ZnO	0.04										
CaO		0.26	0.29	22.23	23.26	25.31	12.31	12.17	0.08	36.89	0.95
Na_2O			0.03	0.47	0.54	0.04	2.86	2.97	5.52	0.01	18.60
K_2O			0.01				0.14	0.07	0.57		0.17
NiO	0.15	0.31	0.06	0.05	0.02		0.14	0.14	0.24		0.03
Sum Ox%	99.12	100.93	100.12	99.19	99.61	100.60	97.18	97.66	96.03	100.25	100.71
Fo / XMg	59.3	88.6	92.6	93.7	93.8	97.0	92.4	92.7	95.0		
XCr	51.6										
YFe^{3+}	3.11										
XNa							96.8	98.5	93.6		